Magnetoelastic modes and lifetime of magnons in thin yttrium iron garnet films

Andreas Rückriegel and Peter Kopietz
Institut für Theoretische Physik, Universität Frankfurt, Max-von-Laue Strasse 1, 60438 Frankfurt, Germany
and Department of Physics, University of Florida, Gainesville, Florida 32611, USA

Dmytro A. Bozhko, Alexander A. Serga, and Burkard Hillebrands
Fachbereich Physik and Landesforschungszentrum OPTIMAS, Technische Universität Kaiserslautern, 67663 Kaiserslautern, Germany
(Received 12 March 2014; revised manuscript received 5 May 2014; published 20 May 2014)

We calculate the effects of the spin-lattice coupling on the magnon spectrum of thin ferromagnetic films consisting of the magnetic insulator yttrium iron garnet. The magnon-phonon hybridization generates a characteristic minimum in the spin dynamic structure factor which quantitatively agrees with recent Brillouin light scattering experiments. We also show that at room temperature the phonon contribution to the magnon damping exhibits a rather complicated momentum dependence: In the exchange regime the magnon damping is dominated by Cherenkov type scattering processes, while in the long-wavelength dipolar regime these processes are subdominant and the magnon damping is two orders of magnitude smaller. We supplement our calculations by actual measurements of the magnon relaxation in the dipolar regime. Our theory provides a simple explanation of a recent experiment probing the different temperatures of the magnon and phonon gases in yttrium iron garnet.

DOI: 10.1103/PhysRevB.89.184413 PACS number(s): 05.30.Jp, 75.10.Jm, 75.30.Ds

I. INTRODUCTION

Although the spin-lattice interactions in magnetic insulators can often be ignored, in some cases the coupling between the spin degrees of freedom and the lattice vibrations (phonons) plays a crucial role. For example, in ultrasound experiments one uses the spin-lattice coupling to study the properties of the spin degrees of freedom from the measurement of the propagation and the attenuation of sound waves [1]. The theory of magnetoelastic effects in magnetic insulators has been developed more than half a century ago by Abrahams and Kittel [2,3], and by Kaganov and Tsukernik [4]. While in the past decades a few theoretical studies of magnetoelastic effects have appeared [5–10], recent experimental progress in the field of spintronics has revived the interest in the interactions between spin and lattice degrees of freedom [11].

The present work is motivated by an experiment [12] where the coupling between magnons and phonons in the magnetic insulator yttrium iron garnet (YIG) was probed via a spatially resolved measurement of the magnon temperature T_m in the presence of a thermal gradient. In the short wavelength exchange part of the magnon spectrum T_m was found to agree almost perfectly with the temperature T_p of the phonon bath. In order to reconcile this finding with earlier studies of the spin Seebeck effect [13] (which relies on the difference between T_m and T_p), the authors of Ref. [12] speculated that in the long-wavelength dipolar part of the spectrum the magnon temperature significantly differs from T_p, suggesting a rather weak coupling between magnons and phonons in this regime. In this work we offer a microscopic explanation for such a momentum dependence of the magnon temperature: We show that the lifetime $\tau(\boldsymbol{k})$ of magnons due to coupling to the phonons in YIG is strongly momentum dependent; in particular $\tau(\boldsymbol{k})$ exhibits a pronounced minimum in the exchange regime and is two orders of magnitude larger in the dipolar regime. Since in the dipolar part of the spectrum the magnons have a longer lifetime, in this regime phonons are less effective to thermalize the magnons and the differences between T_m and T_p can persist for longer times.

We also present experimental results for the magnon damping in the dipolar regime, which have been obtained by means of time- and wave-vector-resolved Brillouin light scattering (BLS) spectroscopy [14]. The experimentally determined damping rate is three orders of magnitude larger than our theoretical prediction, although the qualitative behavior as a function of in-plane momentum is similar. One should keep in mind, however, that in our calculations only the relaxation due to magnon-phonon interactions has been taken into account. Apparently, in the long-wavelength dipolar regime other scattering channels leading to momentum relaxation are dominant, such as elastic magnon-impurity scattering.

The rest of this work is organized as follows: In Sec. II we briefly review the calculation of the spin wave spectrum of a thin YIG stripe and fix the experimentally relevant parameters. In Sec. III we carefully derive the magnon-phonon interaction by quantizing the phenomenological classical magnetoelastic energy. The calculation of the magnetoelastic modes due to the magnon-phonon hybridization is presented in Sec. IV. We also calculate the resulting spectral function of the magnons and the transverse dynamic structure factor which is proportional to the BLS cross section. Since we are interested in the magnon dynamics, we derive the effective action of the magnons by integrating over the phonon degrees of freedom. Using this effective action, we proceed in Sec. V to calculate the damping of the magnons due to the coupling to the phonons. We also present new experimental results for the magnon damping in the long-wavelength dipolar regime, and compare them to our calculations. Finally, in Sec. VI we present our conclusions. To make contact with previous work [9] on magnon-phonon interactions in YIG, we present in the Appendix an alternative derivation of the dispersion of the magnetoelastic modes using the equations of motion.

II. MAGNONS IN YIG

It is generally established that the magnetic properties of YIG at room temperature can be obtained from the following

effective quantum spin Hamiltonian [15–17]:

$$\mathcal{H} = -\frac{1}{2}\sum_{ij}\sum_{\alpha\beta}\left(J_{ij}\delta_{\alpha\beta} + D_{ij}^{\alpha\beta}\right)S_i^\alpha S_j^\beta - h\sum_i S_i^z, \quad (2.1)$$

where the spin operators $\boldsymbol{S}_i = \boldsymbol{S}(\boldsymbol{R}_i)$ are localized at the sites $\boldsymbol{R}_i$ of a cubic lattice with lattice spacing $a \approx 12.376$ Å, the exchange couplings $J_{ij} = J(\boldsymbol{R}_i - \boldsymbol{R}_j)$ connect the spins at nearest neighbor sites $\boldsymbol{R}_i$ and $\boldsymbol{R}_j$, and $h = \mu H$ is the Zeeman energy due to an external magnetic field H along the z axis (where $\mu = 2\mu_B$, and μ_B is the Bohr magneton). The dipole-dipole interaction is

$$D_{ij}^{\alpha\beta} = (1-\delta_{ij})\frac{\mu^2}{|\boldsymbol{R}_{ij}|^3}\left[3\hat{R}_{ij}^\alpha \hat{R}_{ij}^\beta - \delta_{\alpha\beta}\right], \quad (2.2)$$

where $\boldsymbol{R}_{ij} = \boldsymbol{R}_i - \boldsymbol{R}_j$ and $\hat{\boldsymbol{R}}_{ij} = \boldsymbol{R}_{ij}/|\boldsymbol{R}_{ij}|$. Within the framework of the usual expansion in inverse powers of the spin S the low-energy magnon spectrum of YIG can be quantitatively described if one chooses $J \approx 3.19$ K and $S = M_s a^3/\mu \approx 14.2$, where the saturation magnetization of YIG is given by $4\pi M_s = 1750$ G. Due to the large value of the effective spin S we may use the Holstein-Primakoff transformation [18] to express the spin operators in terms of canonical boson operators b_i and $b_i^\dagger$ and expand the square roots,

$$S_i^+ = \sqrt{2S}\sqrt{1-\frac{b_i^\dagger b_i}{2S}}\,b_i \approx \sqrt{2S}\left[b_i - \frac{b_i^\dagger b_i b_i}{4S}\right], \quad (2.3a)$$

$$S_i^- = \sqrt{2S}b_i^\dagger\sqrt{1-\frac{b_i^\dagger b_i}{2S}} \approx \sqrt{2S}\left[b_i^\dagger - \frac{b_i^\dagger b_i^\dagger b_i}{4S}\right], \quad (2.3b)$$

$$S_i^z = S - b_i^\dagger b_i, \quad (2.3c)$$

where $S_i^+ = S_i^x + iS_i^y$ and $S_i^- = S_i^x - iS_i^y$, and we have assumed that the magnetization of the system is uniform and points along the z axis. To describe a thin stripe we can work with an effective two-dimensional model, as explained in Ref. [17]. In the geometry shown in Fig. 1 the in-plane magnon wave vectors are then of the form $\boldsymbol{k} = k_y\boldsymbol{e}_y + k_z\boldsymbol{e}_z = |\boldsymbol{k}|\cos\theta_{\boldsymbol{k}}\boldsymbol{e}_z + |\boldsymbol{k}|\sin\theta_{\boldsymbol{k}}\boldsymbol{e}_y$. Defining

$$b_{\boldsymbol{k}} = \frac{1}{\sqrt{N}}\sum_i e^{-i\boldsymbol{k}\cdot\boldsymbol{R}_i}b_i, \quad (2.4)$$

where N denotes the number of lattice sites in the yz plane, and retaining only quadratic terms in the bosons, we obtain

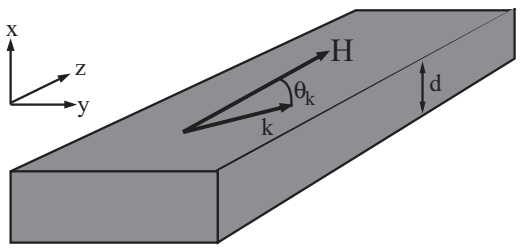

FIG. 1. Thin YIG stripe of thickness d in a magnetic field $\boldsymbol{H} = H\boldsymbol{e}_z$ along the direction $\boldsymbol{e}_z$ of the long axis. We consider magnons with wave vector $\boldsymbol{k} = |\boldsymbol{k}|\cos\theta_{\boldsymbol{k}}\boldsymbol{e}_z + |\boldsymbol{k}|\sin\theta_{\boldsymbol{k}}\boldsymbol{e}_y$ in the stripe plane.

the bosonized Hamiltonian for YIG,

$$\mathcal{H}_{\rm m}^{(2)} = \sum_{\boldsymbol{k}}\left[A_{\boldsymbol{k}}b_{\boldsymbol{k}}^\dagger b_{\boldsymbol{k}} + \frac{B_{\boldsymbol{k}}}{2}(b_{\boldsymbol{k}}^\dagger b_{-\boldsymbol{k}}^\dagger + b_{-\boldsymbol{k}}b_{\boldsymbol{k}})\right]. \quad (2.5)$$

Here the energies $A_{\boldsymbol{k}}$ and $B_{\boldsymbol{k}}$ can be expressed in terms of the Fourier transforms $J_{\boldsymbol{k}}$ and $D_{\boldsymbol{k}}^{\alpha\beta}$ of the exchange couplings and the dipole-dipole interaction as [17]

$$A_{\boldsymbol{k}} = h + S(J_0 - J_{\boldsymbol{k}}) + S\left(D_0^{zz} - \frac{D_{\boldsymbol{k}}^{xx} + D_{\boldsymbol{k}}^{yy}}{2}\right), \quad (2.6a)$$

$$B_{\boldsymbol{k}} = -S\frac{D_{\boldsymbol{k}}^{xx} - D_{\boldsymbol{k}}^{yy}}{2}. \quad (2.6b)$$

The Hamiltonian (2.5) is easily diagonalized by means of a Bogoliubov transformation,

$$\begin{pmatrix} b_{\boldsymbol{k}} \\ b_{-\boldsymbol{k}}^\dagger \end{pmatrix} = \begin{pmatrix} u_{\boldsymbol{k}} & -v_{\boldsymbol{k}} \\ -v_{\boldsymbol{k}}^* & u_{\boldsymbol{k}} \end{pmatrix}\begin{pmatrix} \beta_{\boldsymbol{k}} \\ \beta_{-\boldsymbol{k}}^\dagger \end{pmatrix}, \quad (2.7)$$

with

$$u_{\boldsymbol{k}} = \sqrt{\frac{A_{\boldsymbol{k}} + E_{\boldsymbol{k}}}{2E_{\boldsymbol{k}}}}, \quad v_{\boldsymbol{k}} = \frac{B_{\boldsymbol{k}}}{|B_{\boldsymbol{k}}|}\sqrt{\frac{A_{\boldsymbol{k}} - E_{\boldsymbol{k}}}{2E_{\boldsymbol{k}}}}, \quad (2.8)$$

and

$$E_{\boldsymbol{k}} = \sqrt{A_{\boldsymbol{k}}^2 - B_{\boldsymbol{k}}^2}. \quad (2.9)$$

In terms of the magnon quasiparticle operators $\beta_{\boldsymbol{k}}$ the Hamiltonian is diagonal,

$$\mathcal{H}_{\rm m}^{(2)} = \sum_{\boldsymbol{k}}\left[E_{\boldsymbol{k}}\beta_{\boldsymbol{k}}^\dagger\beta_{\boldsymbol{k}} + \frac{A_{\boldsymbol{k}} - E_{\boldsymbol{k}}}{2E_{\boldsymbol{k}}}\right]. \quad (2.10)$$

For a thin stripe with thickness d the magnon dispersion can be approximated for small wave vectors by [17,19]

$$E_{\boldsymbol{k}} = [h + \rho_s\boldsymbol{k}^2 + \Delta(1-f_{\boldsymbol{k}})\sin^2\theta_{\boldsymbol{k}}]^{1/2} \times [h + \rho_s\boldsymbol{k}^2 + \Delta f_{\boldsymbol{k}}]^{1/2}, \quad (2.11)$$

where $\theta_{\boldsymbol{k}}$ is the angle between the magnetic field and the wave vector $\boldsymbol{k}$ and the form factor can be approximated by

$$f_{\boldsymbol{k}} \approx \frac{1 - e^{-|\boldsymbol{k}|d}}{|\boldsymbol{k}|d}. \quad (2.12)$$

For a thin YIG stripe the exchange spin stiffness ρ_s and the dipolar energy scale Δ have the values [9,20]

$$\rho_s = 2\mu_B \times 5.17 \times 10^{-9}\ \text{Oe cm}^2 \approx 945\ \text{GHz} \times a^2 \times 2\pi\hbar, \quad (2.13)$$

$$\Delta = 3SD_0^{zz} = 2\mu_B \times 4\pi M_s = 2\mu_B \times 1750\ \text{G} \approx 0.235\ \text{K} \times k_B = 4.89\ \text{GHz} \times 2\pi\hbar. \quad (2.14)$$

Note that in units where $k_B = 1$ and $h = 2\pi\hbar = 1$ we have $1\ \text{K} \approx 20.8$ GHz.

III. MAGNON-PHONON HAMILTONIAN OF THIN YIG FILMS

One source of the spin-phonon coupling is the dependence of the true positions $\boldsymbol{r}_i = \boldsymbol{R}_i + \boldsymbol{X}_i$ of the spins on the

phonon displacements $\boldsymbol{X}_i = \boldsymbol{X}(\boldsymbol{R}_i)$ at the lattice sites $\boldsymbol{R}_i$. The resulting magnon phonon interaction can be derived from the effective spin-model (2.1) by expanding the exchange couplings $J_{ij} = J(\boldsymbol{R}_i - \boldsymbol{R}_i + \boldsymbol{X}_i - \boldsymbol{X}_j)$ in powers of the phonon displacements [21]. However, in collinear magnets such a procedure does not take into account the dominant source of the magnon-phonon interaction, which is generated by relativistic effects such as dipole-dipole interactions and spin-orbit coupling [9]. These effects involve the charge degrees of freedom so that they cannot be simply included in our effective spin model (2.1). To derive the proper quantized interaction between magnons and phonons in YIG, we therefore follow the semiphenomenological approach pioneered by Abrahams and Kittel [2], which relies on the quantization of the phenomenological expression for the classical magnetoelastic energy.

A. Classical magnetoelastic energy in YIG

To second order in the spin-density field $\boldsymbol{M}(\boldsymbol{r})$ and to first order in the displacement field $\boldsymbol{X}(\boldsymbol{r})$ associated with long-wavelength acoustic phonons the phenomenological expression for the magnetoelastic energy is [2–4,7,9]

$$E_{\rm me}[\boldsymbol{M},\boldsymbol{X}] = \frac{n}{M_s^2}\int d^3r \sum_{\alpha\beta}\Bigg[B_{\alpha\beta}M_\alpha(\boldsymbol{r})M_\beta(\boldsymbol{r}) + B'_{\alpha\beta}\frac{\partial \boldsymbol{M}(\boldsymbol{r})}{\partial r_\alpha}\frac{\partial \boldsymbol{M}(\boldsymbol{r})}{\partial r_\beta}\Bigg]X_{\alpha\beta}(\boldsymbol{r}), \tag{3.1}$$

where $\boldsymbol{M}(\boldsymbol{r})$ is the local magnetization (i.e., the magnetic moment per unit volume at position $\boldsymbol{r}$), M_s is the saturation magnetization, $n = N/V$ is the number density of the magnetic particles in the system, and

$$X_{\alpha\beta}(\boldsymbol{r}) = \frac{1}{2}\left[\frac{\partial X_\alpha(\boldsymbol{r})}{\partial r_\beta} + \frac{\partial X_\beta(\boldsymbol{r})}{\partial r_\alpha}\right] \tag{3.2}$$

is the symmetric strain tensor. Here $X_\alpha(\boldsymbol{r}) = \boldsymbol{e}_\alpha \cdot \boldsymbol{X}(\boldsymbol{r})$ are the projections of the phonon displacement field $\boldsymbol{X}(\boldsymbol{r})$ onto the cartesian unit vectors $\boldsymbol{e}_\alpha$, where $\alpha = x,y,z$. The first term on the right-hand side of Eq. (3.1) involving the couplings $B_{\alpha\beta}$ is due to relativistic effects such as dipole-dipole interactions and spin-orbit coupling, while the gradient term involving $B'_{\alpha\beta}$ is generated by the dependence of the exchange interaction on the phonon coordinates. For a cubic lattice the phenomenological coupling tensors $B_{\alpha\beta}$ and $B'_{\alpha\beta}$ have the structure

$$B_{\alpha\beta} = \delta_{\alpha\beta}B_\parallel + (1-\delta_{\alpha\beta})B_\perp, \tag{3.3a}$$

$$B'_{\alpha\beta} = \delta_{\alpha\beta}B'_\parallel + (1-\delta_{\alpha\beta})B'_\perp. \tag{3.3b}$$

The prefactor of n/M_s^2 in Eq. (3.1) is introduced such that $B_\perp$ and $B_\parallel$ have units of energy. Transforming to wave vector space,

$$\boldsymbol{M}(\boldsymbol{r}) = \int_{\boldsymbol{k}} e^{i\boldsymbol{k}\cdot\boldsymbol{r}}\boldsymbol{M}(\boldsymbol{k}), \tag{3.4a}$$

$$\boldsymbol{X}(\boldsymbol{r}) = \int_{\boldsymbol{k}} e^{i\boldsymbol{k}\cdot\boldsymbol{r}}\boldsymbol{X}(\boldsymbol{k}), \tag{3.4b}$$

$$X_{\alpha\beta}(\boldsymbol{r}) = \int_{\boldsymbol{k}} e^{i\boldsymbol{k}\cdot\boldsymbol{r}}X_{\alpha\beta}(\boldsymbol{k}), \tag{3.4c}$$

where $\int_{\boldsymbol{k}} = \int \frac{d^3k}{(2\pi)^3}$, the matrix elements of the strain tensor in Fourier space are

$$X_{\alpha\beta}(\boldsymbol{k}) = \frac{i}{2}[X_\alpha(\boldsymbol{k})k_\beta + X_\beta(\boldsymbol{k})k_\alpha], \tag{3.5}$$

and the magnetoelastic energy can be written as

$$E_{\rm me}[\boldsymbol{M},\boldsymbol{X}] = \frac{n}{M_s^2}\int_{\boldsymbol{k}}\int_{\boldsymbol{k}'}\int_{\boldsymbol{q}}(2\pi)^3\delta(\boldsymbol{k}+\boldsymbol{k}'+\boldsymbol{q})\sum_{\alpha\beta}[B_{\alpha\beta}M_\alpha(\boldsymbol{k})M_\beta(\boldsymbol{k}') - B'_{\alpha\beta}k_\alpha k'_\beta \boldsymbol{M}(\boldsymbol{k})\cdot\boldsymbol{M}(\boldsymbol{k}')]X_{\alpha\beta}(\boldsymbol{q}). \tag{3.6}$$

At long wavelength the dominant contribution to the magnetoelastic coupling is due to spin-orbit coupling [9] so that in this work we shall neglect the exchange contribution, setting $B'_{\alpha\beta} = 0$. For YIG at room temperature the numerical values for the magnetoelastic coupling constants are [9,22,23]

$$nB_\parallel = 3.48\times10^6\ \text{erg/cm}^3, \quad nB_\perp = 6.96\times10^6\ \text{erg/cm}^3. \tag{3.7}$$

The number density of the magnetic ions in YIG is [20]

$$n = 1/a^3, \quad a = 12.376\ \text{Å}, \tag{3.8}$$

so that in units where the Boltzmann constant and $2\pi\hbar$ are set equal to unity

$$B_\parallel = 47.8\ \text{K} = 994\ \text{GHz}, \qquad B_\perp = 95.6\ \text{K} = 1988\ \text{GHz}. \tag{3.9}$$

B. Quantized magnon-phonon interaction in the Holstein-Primakoff basis

Let us now quantize the magnetoelastic energy. For the phonon field we adopt the usual strategy of expressing the displacement field by the bosonic creation and annihilation operators $a^\dagger_{\boldsymbol{k}\lambda}$ and $a_{\boldsymbol{k}\lambda}$ of the phonon eigenmodes with momentum $\boldsymbol{k}$ and polarization $\boldsymbol{e}_{\boldsymbol{k}\lambda}$,

$$\boldsymbol{X}(\boldsymbol{k}) \to \frac{V}{\sqrt{N}}\boldsymbol{X}_{\boldsymbol{k}}, \tag{3.10}$$

$$\boldsymbol{X}_{\boldsymbol{k}} = \sum_\lambda X_{\boldsymbol{k}\lambda}\boldsymbol{e}_{\boldsymbol{k}\lambda} = \sum_\lambda \frac{a_{\boldsymbol{k}\lambda} + a^\dagger_{-\boldsymbol{k}\lambda}}{\sqrt{2m\omega_{\boldsymbol{k}\lambda}}}\boldsymbol{e}_{\boldsymbol{k}\lambda}, \tag{3.11}$$

where $\lambda = 1,2,3$ labels the three acoustic phonon branches, $\omega_{\boldsymbol{k}\lambda} = c_\lambda|\boldsymbol{k}|$ are the phonon dispersions, m is the effective ionic mass in a unit cell, V is the volume of the system, and N is the number of unit cells. Note that in general the polarization vectors satisfy [24] the orthogonality relations $\boldsymbol{e}^*_{\boldsymbol{k}\lambda}\cdot\boldsymbol{e}_{\boldsymbol{k}\lambda'} = \delta_{\lambda\lambda'}$ and the completeness relation $\sum_\lambda \boldsymbol{e}_{\boldsymbol{k}\lambda}\boldsymbol{e}^\dagger_{\boldsymbol{k}\lambda} = \mathbf{1}$, so that we may identify

$$X_{\boldsymbol{k}\lambda} = \boldsymbol{e}^*_{\boldsymbol{k}\lambda}\cdot\boldsymbol{X}_{\boldsymbol{k}} = \frac{a_{\boldsymbol{k}\lambda} + a^\dagger_{-\boldsymbol{k}\lambda}}{\sqrt{2m\omega_{\boldsymbol{k}\lambda}}}. \tag{3.12}$$

Below we shall denote the Fourier transform of the quantized strain tensor by

$$X^{\alpha\beta}_{\boldsymbol{k}} = \frac{i}{2}\boldsymbol{k}_{\alpha\beta}\cdot\boldsymbol{X}_{\boldsymbol{k}}, \quad \boldsymbol{k}_{\alpha\beta} = k_\alpha\boldsymbol{e}_\beta + k_\beta\boldsymbol{e}_\alpha. \tag{3.13}$$

We may also choose the phases of the unit vectors such that [24] $\boldsymbol{e}^*_{\boldsymbol{k}\lambda} = \boldsymbol{e}_{-\boldsymbol{k}\lambda}$. For a quasi-two-dimensional YIG stripe in the yz plane we parametrize the in-plane wave vectors as $\boldsymbol{k} = |\boldsymbol{k}|(\cos\theta_{\boldsymbol{k}}\boldsymbol{e}_z + \sin\theta_{\boldsymbol{k}}\boldsymbol{e}_y)$, as shown in Fig. 1. A convenient choice for the polarization vectors of the longitudinal and transverse phonons is then

$$\boldsymbol{e}_{\boldsymbol{k}\parallel} = i(\boldsymbol{e}_z\cos\theta_{\boldsymbol{k}} + \boldsymbol{e}_y\sin\theta_{\boldsymbol{k}}), \tag{3.14a}$$

$$\boldsymbol{e}_{\boldsymbol{k}\perp 1} = i(\boldsymbol{e}_z\sin\theta_{\boldsymbol{k}} - \boldsymbol{e}_y\cos\theta_{\boldsymbol{k}}), \tag{3.14b}$$

$$\boldsymbol{e}_{\boldsymbol{k}\perp 2} = \boldsymbol{e}_x. \tag{3.14c}$$

For YIG the relevant value of the effective ionic mass appearing in Eqs. (3.11) and (3.12) is [9,20]

$$m = \rho a^3, \quad \rho = 5.17\ \mathrm{g/cm^3}, \tag{3.15}$$

and the longitudinal and transverse phonon velocities are

$$\begin{aligned} c_\parallel &= 7.209\times 10^5\ \mathrm{cm/s},\\ c_\perp &= 3.843\times 10^5\ \mathrm{cm/s}. \end{aligned} \tag{3.16}$$

To quantize the magnetic sector, we follow Refs. [2–4] and replace the magnetization $\boldsymbol{M}(\boldsymbol{r})$ at lattice site $\boldsymbol{r} = \boldsymbol{R}_i$ by the corresponding spin-operator $\boldsymbol{S}_i$ according to the prescription

$$\boldsymbol{M}(\boldsymbol{R}_i) \to 2\mu_B n\boldsymbol{S}_i, \tag{3.17}$$

where $n = N/V = 1/a^3$ is the number density. In Fourier space Eq. (3.17) corresponds to

$$\boldsymbol{M}(\boldsymbol{k}) \to g\mu_B\sqrt{N}\boldsymbol{S}_{\boldsymbol{k}} = g\mu_B\sum_i e^{-i\boldsymbol{k}\cdot\boldsymbol{R}_i}\boldsymbol{S}_i. \tag{3.18}$$

Assuming that the macroscopic magnetization points along the z axis, we may express the components of the spin operators at lattice site $\boldsymbol{R}_i$ in terms of Holstein-Primakoff bosons (magnons) b_i and $b_i^\dagger$ as usual with Eqs. (2.3a)–(2.3c). In momentum space we have

$$S^z_{\boldsymbol{k}} = \sqrt{N}S\delta_{\boldsymbol{k},0} - \frac{1}{\sqrt{N}}\sum_{\boldsymbol{q}} b^\dagger_{\boldsymbol{q}}b_{\boldsymbol{q}+\boldsymbol{k}}, \tag{3.19}$$

and to leading order in an expansion in powers of $1/S$,

$$S^x_{\boldsymbol{k}} \approx \frac{\sqrt{2S}}{2}(b_{\boldsymbol{k}} + b^\dagger_{-\boldsymbol{k}}), \tag{3.20}$$

$$S^y_{\boldsymbol{k}} \approx \frac{\sqrt{2S}}{2i}(b_{\boldsymbol{k}} - b^\dagger_{-\boldsymbol{k}}). \tag{3.21}$$

For large S it is reasonable to retain only terms up to quadratic order in the magnons, so that the resulting magnetoelastic Hamiltonian can be written as

$$\mathcal{H}_{\mathrm{me}} = \mathcal{H}^{(2)}_{\mathrm{me}} + \mathcal{H}^{(3)}_{\mathrm{me}}, \tag{3.22}$$

where the superscript indicates the number of operators involved. The quadratic term $\mathcal{H}^{(2)}_{\mathrm{me}}$ is

$$\begin{aligned} \mathcal{H}^{(2)}_{\mathrm{me}} &= B_\perp\sqrt{\frac{2}{S}}\sum_{\boldsymbol{k}}\left[X^{zx}_{-\boldsymbol{k}}(b_{\boldsymbol{k}} + b^\dagger_{-\boldsymbol{k}}) - iX^{zy}_{-\boldsymbol{k}}(b_{\boldsymbol{k}} - b^\dagger_{-\boldsymbol{k}})\right]\\ &= \sum_{\boldsymbol{k}}\boldsymbol{X}_{-\boldsymbol{k}}\cdot[\boldsymbol{\Gamma}_{\boldsymbol{k}}b_{\boldsymbol{k}} + \boldsymbol{\Gamma}^*_{-\boldsymbol{k}}b^\dagger_{-\boldsymbol{k}}]\\ &= \sum_{\boldsymbol{k}}[\boldsymbol{X}^*_{\boldsymbol{k}}\cdot\boldsymbol{\Gamma}_{\boldsymbol{k}}b_{\boldsymbol{k}} + \boldsymbol{X}_{\boldsymbol{k}}\cdot\boldsymbol{\Gamma}^*_{\boldsymbol{k}}b^\dagger_{\boldsymbol{k}}], \end{aligned} \tag{3.23}$$

where we have used the fact that the $\boldsymbol{X}_{\boldsymbol{k}}$ are the Fourier components of a hermitian operator so that

$$\boldsymbol{X}_{-\boldsymbol{k}} = \boldsymbol{X}^*_{\boldsymbol{k}}, \tag{3.24}$$

and the vector vertex $\boldsymbol{\Gamma}_{\boldsymbol{k}}$ is defined by

$$\begin{aligned} \boldsymbol{\Gamma}_{\boldsymbol{k}} &= -\frac{B_\perp}{\sqrt{2S}}(\boldsymbol{k}_{yz} + i\boldsymbol{k}_{xz})\\ &= -\frac{B_\perp}{\sqrt{2S}}[(k_y + ik_x)\boldsymbol{e}_z + k_z(\boldsymbol{e}_y + i\boldsymbol{e}_x)]. \end{aligned} \tag{3.25}$$

Expanding

$$\boldsymbol{X}_{\boldsymbol{k}} = \sum_\lambda X_{\boldsymbol{k}\lambda}\boldsymbol{e}_{\boldsymbol{k}\lambda}, \quad \boldsymbol{\Gamma}_{\boldsymbol{k}} = \sum_\lambda \Gamma_{\boldsymbol{k}\lambda}\boldsymbol{e}_{\boldsymbol{k}\lambda}, \tag{3.26}$$

with

$$X_{\boldsymbol{k}\lambda} = \boldsymbol{e}^*_{\boldsymbol{k}\lambda}\cdot\boldsymbol{X}_{\boldsymbol{k}}, \quad \Gamma_{\boldsymbol{k}\lambda} = \boldsymbol{e}^*_{\boldsymbol{k}\lambda}\cdot\boldsymbol{\Gamma}_{\boldsymbol{k}}, \tag{3.27}$$

the Hamiltonian (3.23) can be written as

$$\begin{aligned} \mathcal{H}^{(2)}_{\mathrm{me}} &= \sum_{\boldsymbol{k}\lambda}[\Gamma_{\boldsymbol{k}\lambda}X^*_{\boldsymbol{k}\lambda}b_{\boldsymbol{k}} + \Gamma^*_{\boldsymbol{k}\lambda}X_{\boldsymbol{k}\lambda}b^\dagger_{\boldsymbol{k}}]\\ &= \sum_{\boldsymbol{k}\lambda}X_{-\boldsymbol{k}\lambda}[\Gamma_{\boldsymbol{k}\lambda}b_{\boldsymbol{k}} + \Gamma^*_{-\boldsymbol{k}\lambda}b^\dagger_{-\boldsymbol{k}}]. \end{aligned} \tag{3.28}$$

This part of the magnetoelastic Hamiltonian describes the hybridization between the phonon and magnon degrees of freedom. With the choice (3.14a)–(3.14c) of the phonon basis we obtain for the projections of the hybridization vertex

$$\Gamma_{\boldsymbol{k}\parallel} = i\frac{B_\perp}{\sqrt{2S}}\frac{2k_yk_z}{|\boldsymbol{k}|} = i\frac{B_\perp}{\sqrt{2S}}|\boldsymbol{k}|\sin(2\theta_{\boldsymbol{k}}), \tag{3.29a}$$

$$\Gamma_{\boldsymbol{k}\perp 1} = i\frac{B_\perp}{\sqrt{2S}}\frac{k_y^2 - k_z^2}{|\boldsymbol{k}|} = -i\frac{B_\perp}{\sqrt{2S}}|\boldsymbol{k}|\cos(2\theta_{\boldsymbol{k}}), \tag{3.29b}$$

$$\Gamma_{\boldsymbol{k}\perp 2} = -i\frac{B_\perp}{\sqrt{2S}}k_z = -i\frac{B_\perp}{\sqrt{2S}}|\boldsymbol{k}|\cos\theta_{\boldsymbol{k}}. \tag{3.29c}$$

Before discussing the spectrum of the magnetoelastic modes, let us write down the cubic term $\mathcal{H}^{(3)}_{\mathrm{me}}$ of the magnetoelastic Hamiltonian in the form [21]

$$\begin{aligned} \mathcal{H}^{(3)}_{\mathrm{me}} &= \frac{1}{\sqrt{N}}\sum_{\boldsymbol{k}\boldsymbol{k}'}\Big[\boldsymbol{\Gamma}^{\bar{b}b}_{\boldsymbol{k},\boldsymbol{k}'}\cdot\boldsymbol{X}_{\boldsymbol{k}-\boldsymbol{k}'}b^\dagger_{\boldsymbol{k}}b_{\boldsymbol{k}'}\\ &\quad + \frac{1}{2!}\left(\boldsymbol{\Gamma}^{bb}_{\boldsymbol{k},\boldsymbol{k}'}\cdot\boldsymbol{X}_{-\boldsymbol{k}-\boldsymbol{k}'}b_{\boldsymbol{k}}b_{\boldsymbol{k}'} + \boldsymbol{\Gamma}^{\bar{b}\bar{b}}_{\boldsymbol{k},\boldsymbol{k}'}\cdot\boldsymbol{X}_{\boldsymbol{k}+\boldsymbol{k}'}b^\dagger_{\boldsymbol{k}}b^\dagger_{\boldsymbol{k}'}\right)\Big]\\ &= \frac{1}{\sqrt{N}}\sum_{\boldsymbol{k}\boldsymbol{q}}\boldsymbol{X}_{-\boldsymbol{q}}\cdot\Big[\boldsymbol{U}_{-\boldsymbol{q}}b^\dagger_{\boldsymbol{k}}b_{\boldsymbol{k}+\boldsymbol{q}}\\ &\quad + \frac{1}{2!}\left(\boldsymbol{V}_{-\boldsymbol{q}}b_{-\boldsymbol{k}}b_{\boldsymbol{k}+\boldsymbol{q}} + \boldsymbol{V}^*_{\boldsymbol{q}}b^\dagger_{\boldsymbol{k}}b^\dagger_{-\boldsymbol{k}-\boldsymbol{q}}\right)\Big], \end{aligned} \tag{3.30}$$

where the vector vertices are given by

$$\boldsymbol{\Gamma}^{\bar{b}b}_{\boldsymbol{k},\boldsymbol{k}'} = \boldsymbol{U}_{\boldsymbol{k}-\boldsymbol{k}'}, \tag{3.31a}$$

$$\boldsymbol{\Gamma}^{bb}_{\boldsymbol{k},\boldsymbol{k}'} = \boldsymbol{V}_{\boldsymbol{k}+\boldsymbol{k}'}, \tag{3.31b}$$

$$\boldsymbol{\Gamma}^{\bar{b}\bar{b}}_{\boldsymbol{k},\boldsymbol{k}'} = \boldsymbol{V}^*_{-\boldsymbol{k}-\boldsymbol{k}'}, \tag{3.31c}$$

with

$$\boldsymbol{U}_{\boldsymbol{q}} = \frac{i B_{\parallel}}{S}(q_x \boldsymbol{e}_x + q_y \boldsymbol{e}_y - 2q_z \boldsymbol{e}_z), \tag{3.32a}$$

$$\boldsymbol{V}_{\boldsymbol{q}} = \frac{i B_{\parallel}}{S}(q_x \boldsymbol{e}_x - q_y \boldsymbol{e}_y) + \frac{B_{\perp}}{S}\boldsymbol{q}_{xy} = \frac{i B_{\parallel}}{S}(q_x \boldsymbol{e}_x - q_y \boldsymbol{e}_y) + \frac{B_{\perp}}{S}(q_x \boldsymbol{e}_y + q_y \boldsymbol{e}_x). \tag{3.32b}$$

C. Magnetoelastic interaction vertices in the quasiparticle basis

For the calculation of the spectral function of the magnons it is useful to express the magnetoelastic interaction in terms of the magnon quasiparticle operators $\beta_{\boldsymbol{k}}$ and $\beta^{\dagger}_{\boldsymbol{k}}$ which are related to the Holstein-Primakoff bosons $b_{\boldsymbol{k}}$ and $b^{\dagger}_{\boldsymbol{k}}$ via the Bogoliubov transformation (2.7). Substituting this transformation into Eqs. (3.23) and (3.30) we obtain for the hybridization part

$$\mathcal{H}^{(2)}_{\mathrm{me}} = \sum_{\boldsymbol{k}\lambda} X_{-\boldsymbol{k}\lambda}\left[\Gamma^{\beta}_{\boldsymbol{k}\lambda}\beta_{\boldsymbol{k}} + \Gamma^{\bar{\beta}}_{-\boldsymbol{k}\lambda}\beta^{\dagger}_{-\boldsymbol{k}}\right], \tag{3.33}$$

with

$$\Gamma^{\beta}_{\boldsymbol{k}\lambda} = u_{\boldsymbol{k}}\Gamma_{\boldsymbol{k}\lambda} - v^{*}_{\boldsymbol{k}}\Gamma^{*}_{-\boldsymbol{k}\lambda}, \tag{3.34}$$

$$\Gamma^{\bar{\beta}}_{\boldsymbol{k}\lambda} = u_{\boldsymbol{k}}\Gamma^{*}_{\boldsymbol{k}\lambda} - v_{\boldsymbol{k}}\Gamma_{-\boldsymbol{k}\lambda} = \left(\Gamma^{\beta}_{\boldsymbol{k}\lambda}\right)^{*}. \tag{3.35}$$

The magnon-phonon interaction defined in Eq. (3.30) can be written as

$$\mathcal{H}^{(3)}_{\mathrm{me}} = \frac{1}{\sqrt{N}}\sum_{\boldsymbol{k}\boldsymbol{k}'}\left[\boldsymbol{\Gamma}^{\bar{\beta}\beta}_{\boldsymbol{k},\boldsymbol{k}'}\cdot\boldsymbol{X}_{\boldsymbol{k}-\boldsymbol{k}'}\beta^{\dagger}_{\boldsymbol{k}}\beta_{\boldsymbol{k}'} + \frac{1}{2!}\left(\boldsymbol{\Gamma}^{\beta\beta}_{\boldsymbol{k},\boldsymbol{k}'}\cdot\boldsymbol{X}_{-\boldsymbol{k}-\boldsymbol{k}'}\beta_{\boldsymbol{k}}\beta_{\boldsymbol{k}'} + \boldsymbol{\Gamma}^{\bar{\beta}\bar{\beta}}_{\boldsymbol{k},\boldsymbol{k}'}\cdot\boldsymbol{X}_{\boldsymbol{k}+\boldsymbol{k}'}\beta^{\dagger}_{\boldsymbol{k}}\beta^{\dagger}_{\boldsymbol{k}'}\right)\right], \tag{3.36}$$

with

$$\begin{aligned}\boldsymbol{\Gamma}^{\bar{\beta}\beta}_{\boldsymbol{k},\boldsymbol{k}'} &= u_{\boldsymbol{k}}u_{\boldsymbol{k}'}\boldsymbol{\Gamma}^{\bar{b}b}_{\boldsymbol{k},\boldsymbol{k}'} + v_{\boldsymbol{k}}v^{*}_{\boldsymbol{k}'}\boldsymbol{\Gamma}^{\bar{b}b}_{-\boldsymbol{k}',-\boldsymbol{k}} - v_{\boldsymbol{k}}u_{\boldsymbol{k}'}\boldsymbol{\Gamma}^{bb}_{-\boldsymbol{k},\boldsymbol{k}'} - u_{\boldsymbol{k}}v^{*}_{\boldsymbol{k}'}\boldsymbol{\Gamma}^{\bar{b}\bar{b}}_{\boldsymbol{k},-\boldsymbol{k}'} \\ &= (u_{\boldsymbol{k}}u_{\boldsymbol{k}'} + v_{\boldsymbol{k}}v^{*}_{\boldsymbol{k}'})\boldsymbol{U}_{\boldsymbol{k}-\boldsymbol{k}'} - v_{\boldsymbol{k}}u_{\boldsymbol{k}'}\boldsymbol{V}_{\boldsymbol{k}'-\boldsymbol{k}} - u_{\boldsymbol{k}}v^{*}_{\boldsymbol{k}'}\boldsymbol{V}^{*}_{\boldsymbol{k}'-\boldsymbol{k}},\end{aligned} \tag{3.37a}$$

$$\begin{aligned}\boldsymbol{\Gamma}^{\beta\beta}_{\boldsymbol{k},\boldsymbol{k}'} &= u_{\boldsymbol{k}}u_{\boldsymbol{k}'}\boldsymbol{\Gamma}^{bb}_{\boldsymbol{k},\boldsymbol{k}'} + v^{*}_{\boldsymbol{k}}v^{*}_{\boldsymbol{k}'}\boldsymbol{\Gamma}^{\bar{b}\bar{b}}_{-\boldsymbol{k},-\boldsymbol{k}'} - v^{*}_{\boldsymbol{k}}u_{\boldsymbol{k}'}\boldsymbol{\Gamma}^{\bar{b}b}_{-\boldsymbol{k},\boldsymbol{k}'} - u_{\boldsymbol{k}}v^{*}_{\boldsymbol{k}'}\boldsymbol{\Gamma}^{\bar{b}b}_{-\boldsymbol{k}',\boldsymbol{k}} \\ &= u_{\boldsymbol{k}}u_{\boldsymbol{k}'}\boldsymbol{V}_{\boldsymbol{k}+\boldsymbol{k}'} + v^{*}_{\boldsymbol{k}}v^{*}_{\boldsymbol{k}'}\boldsymbol{V}^{*}_{\boldsymbol{k}+\boldsymbol{k}'} - (v^{*}_{\boldsymbol{k}}u_{\boldsymbol{k}'} + u_{\boldsymbol{k}}v^{*}_{\boldsymbol{k}'})\boldsymbol{U}_{-\boldsymbol{k}-\boldsymbol{k}'},\end{aligned} \tag{3.37b}$$

$$\begin{aligned}\boldsymbol{\Gamma}^{\bar{\beta}\bar{\beta}}_{\boldsymbol{k},\boldsymbol{k}'} &= u_{\boldsymbol{k}}u_{\boldsymbol{k}'}\boldsymbol{\Gamma}^{\bar{b}\bar{b}}_{\boldsymbol{k},\boldsymbol{k}'} + v_{\boldsymbol{k}}v_{\boldsymbol{k}'}\boldsymbol{\Gamma}^{bb}_{-\boldsymbol{k},-\boldsymbol{k}'} - u_{\boldsymbol{k}}v_{\boldsymbol{k}'}\boldsymbol{\Gamma}^{\bar{b}b}_{\boldsymbol{k},-\boldsymbol{k}'} - v_{\boldsymbol{k}}u_{\boldsymbol{k}'}\boldsymbol{\Gamma}^{\bar{b}b}_{\boldsymbol{k}',-\boldsymbol{k}} \\ &= u_{\boldsymbol{k}}u_{\boldsymbol{k}'}\boldsymbol{V}^{*}_{-\boldsymbol{k}-\boldsymbol{k}'} + v_{\boldsymbol{k}}v_{\boldsymbol{k}'}\boldsymbol{V}_{-\boldsymbol{k}-\boldsymbol{k}'} - (u_{\boldsymbol{k}}v_{\boldsymbol{k}'} + v_{\boldsymbol{k}}u_{\boldsymbol{k}'})\boldsymbol{U}_{\boldsymbol{k}+\boldsymbol{k}'}.\end{aligned} \tag{3.37c}$$

Note that the hermiticity of the Hamiltonian implies

$$\boldsymbol{\Gamma}^{\bar{\beta}\beta}_{\boldsymbol{k},\boldsymbol{k}'} = \left(\boldsymbol{\Gamma}^{\bar{\beta}\beta}_{\boldsymbol{k}',\boldsymbol{k}}\right)^{*}, \quad \boldsymbol{\Gamma}^{\beta\beta}_{\boldsymbol{k},\boldsymbol{k}'} = \left(\boldsymbol{\Gamma}^{\bar{\beta}\bar{\beta}}_{\boldsymbol{k},\boldsymbol{k}'}\right)^{*}. \tag{3.38}$$

Below we shall need these interaction vertices to calculate the damping of the magnons in YIG due to the coupling to the phonons. In fact, we shall need the projections of the three-legged vertices onto the phonon basis, which we define by

$$\Gamma^{\bar{\beta}\beta}_{\boldsymbol{k},\boldsymbol{k}',\lambda} = \boldsymbol{e}^{*}_{\boldsymbol{k}'-\boldsymbol{k},\lambda}\cdot\boldsymbol{\Gamma}^{\bar{\beta}\beta}_{\boldsymbol{k},\boldsymbol{k}'}, \tag{3.39a}$$

$$\Gamma^{\beta\beta}_{\boldsymbol{k},\boldsymbol{k}',\lambda} = \boldsymbol{e}^{*}_{\boldsymbol{k}'+\boldsymbol{k},\lambda}\cdot\boldsymbol{\Gamma}^{\beta\beta}_{\boldsymbol{k},\boldsymbol{k}'}, \tag{3.39b}$$

or in terms of shifted labels,

$$\Gamma^{\bar{\beta}\beta}_{\boldsymbol{k},\boldsymbol{k}+\boldsymbol{q},\lambda} = \boldsymbol{e}^{*}_{\boldsymbol{q},\lambda}\cdot\boldsymbol{\Gamma}^{\bar{\beta}\beta}_{\boldsymbol{k},\boldsymbol{k}+\boldsymbol{q}}, \tag{3.40a}$$

$$\Gamma^{\beta\beta}_{\boldsymbol{k},-\boldsymbol{k}+\boldsymbol{q},\lambda} = \boldsymbol{e}^{*}_{\boldsymbol{q},\lambda}\cdot\boldsymbol{\Gamma}^{\beta\beta}_{\boldsymbol{k},-\boldsymbol{k}+\boldsymbol{q}}. \tag{3.40b}$$

These vertices should also be useful in microscopic calculations of the nonequilibrium dynamics of magnons in YIG. Note that in Ref. [25] only the Cherenkov type of process described by the vertex $\boldsymbol{\Gamma}^{\beta^{\dagger}\beta}_{\boldsymbol{k},\boldsymbol{k}'}$ has been taken into account (however, using a simple phenomenological expression for this vertex). It should be interesting to repeat the calculations of Ref. [25] for the nonequilibrium magnon dynamics in YIG using the more realistic magnon-phonon vertices given above.

IV. MAGNETOELASTIC MODES IN YIG

To calculate the energy dispersion of the magnetoelastic modes, it is sufficient to retain only terms which are quadratic in the magnon and phonon operators. The Hamiltonian of the coupled magnon-phonon system can then be approximated by

$$\mathcal{H}^{(2)} = \mathcal{H}^{(2)}_{\mathrm{m}} + \mathcal{H}^{(2)}_{\mathrm{e}} + \mathcal{H}^{(2)}_{\mathrm{me}}, \tag{4.1}$$

where the quadratic spin wave part $\mathcal{H}^{(2)}_{\mathrm{m}}$ is given in Eqs. (2.5) and (2.10), the pure phonon part can be written as

$$\mathcal{H}^{(2)}_{\mathrm{e}} = \sum_{\boldsymbol{k}\lambda}\left[\frac{P_{-\boldsymbol{k}\lambda}P_{\boldsymbol{k}\lambda}}{2m} + \frac{m}{2}\omega^{2}_{\boldsymbol{k}\lambda}X_{-\boldsymbol{k}\lambda}X_{\boldsymbol{k}\lambda}\right] = \sum_{\boldsymbol{k}\lambda}\omega_{\boldsymbol{k}\lambda}\left[a^{\dagger}_{\boldsymbol{k}\lambda}a_{\boldsymbol{k}\lambda} + \frac{1}{2}\right], \tag{4.2}$$

and the magnon-phonon hybridization $\mathcal{H}^{(2)}_{\mathrm{me}}$ is given in Eqs. (3.28) and (3.33).

A. Effective magnon action and magnon self-energies

To study the effect of the lattice vibrations on the spin excitations, it is convenient to use a functional integral formulation of the coupled magnon-phonon system and integrate over the phonon degrees of freedom, which in our approximation can be done exactly because we have truncated the expansion (3.1) of the magnetoelastic energy at the linear order in the phonon coordinates. The magnon operators $\beta_{\boldsymbol{k}}$ and $\beta^{\dagger}_{\boldsymbol{k}}$ in the quasiparticle basis should then be represented by complex fields β_K and $\bar{\beta}_K$ depending on momentum $\boldsymbol{k}$ and bosonic Matsubara frequency $i\omega$, which we collect into the label $K = (\boldsymbol{k}, i\omega)$. The resulting Euclidean effective action of the magnons is of the form

$$S[\bar{\beta},\beta] = S_2[\bar{\beta},\beta] + S_3[\bar{\beta},\beta] + S_4[\bar{\beta},\beta], \tag{4.3}$$

where the Gaussian part is given by

$$S_2[\bar\beta,\beta] = -\frac{1}{T}\sum_K \Big\{ [i\omega - E_{\boldsymbol k} - \Sigma_1(K)]\bar\beta_K\beta_K - \frac{1}{2}[\Pi_1(K)\beta_{-K}\beta_K + \Pi_1^*(K)\bar\beta_K\bar\beta_{-K}]\Big\}. \quad (4.4)$$

Here the normal and anomalous self-energies to first order in the small parameter $1/S$ are given by

$$\Sigma_1(K) = -\sum_\lambda \frac{|\Gamma^\beta_{\boldsymbol k\lambda}|^2}{m(\omega^2+\omega^2_{\boldsymbol k\lambda})} = -\sum_\lambda |\Gamma^\beta_{\boldsymbol k\lambda}|^2 F_0(K\lambda), \quad (4.5)$$

$$\Pi_1(K) = -\sum_\lambda \frac{\Gamma^\beta_{\boldsymbol k\lambda}\Gamma^\beta_{-\boldsymbol k\lambda}}{m(\omega^2+\omega^2_{\boldsymbol k\lambda})} = -\sum_\lambda \Gamma^\beta_{\boldsymbol k\lambda}\Gamma^\beta_{-\boldsymbol k\lambda} F_0(K\lambda), \quad (4.6)$$

where we have introduced the symmetric phonon propagator

$$F_0(K\lambda) = \frac{1}{m(\omega^2+\omega^2_{\boldsymbol k\lambda})}. \quad (4.7)$$

The interference of the magnon-phonon hybridization with the cubic term of the magnetoelastic coupling yields a cubic contribution to the effective magnon-magnon interaction,

$$S_3[\bar\beta,\beta] = -\frac{1}{T\sqrt{N}}\sum_{K_1K_2K_3}\delta_{K_1+K_2+K_3,0} \times\Big[\frac{1}{2}\Gamma^{\bar\beta\beta\beta}_{1;23}\bar\beta_{-1}\beta_2\beta_3 + \frac{1}{2}\Gamma^{\bar\beta\bar\beta\beta}_{12;3}\bar\beta_{-1}\bar\beta_{-2}\beta_3 + \frac{1}{3!}\Gamma^{\beta\beta\beta}_{123}\beta_1\beta_2\beta_3 + \frac{1}{3!}\Gamma^{\bar\beta\bar\beta\bar\beta}_{123}\bar\beta_{-1}\bar\beta_{-2}\bar\beta_{-3}\Big]. \quad (4.8)$$

Here $\delta_{K,K'} = \delta_{\boldsymbol k,\boldsymbol k'}\delta_{\omega,\omega'}$ and for simplicity we have abbreviated $\beta_1 \equiv \beta_{K_1}$ and $\Gamma^{\bar\beta\beta\beta}_{K_1;K_2K_3} \equiv \Gamma^{\bar\beta\beta\beta}_{1;23}$, and similarly for the other labels. Introducing the notation $F_0(K_1\lambda) = F_{1\lambda}$, the properly symmetrized cubic interaction vertices can be written as

$$\Gamma^{\bar\beta\beta\beta}_{1;23} = \sum_\lambda\big[F_{1\lambda}\Gamma^{\bar\beta}_{-1\lambda}\Gamma^{\beta\beta}_{2,3,\lambda} + F_{2\lambda}\Gamma^{\beta}_{2\lambda}\Gamma^{\bar\beta\beta}_{-1,3,\lambda} + F_{3\lambda}\Gamma^{\beta}_{3\lambda}\Gamma^{\bar\beta\beta}_{-1,2,\lambda}\big], \quad (4.9a)$$

$$\Gamma^{\bar\beta\bar\beta\beta}_{12;3} = \sum_\lambda\big[F_{1\lambda}\Gamma^{\bar\beta}_{-1\lambda}\Gamma^{\bar\beta\beta}_{-2,3,\lambda} + F_{2\lambda}\Gamma^{\bar\beta}_{-2\lambda}\Gamma^{\bar\beta\beta}_{-1,3,\lambda} + F_{3\lambda}\Gamma^{\beta}_{3\lambda}\Gamma^{\bar\beta\bar\beta}_{-1,-2,\lambda}\big], \quad (4.9b)$$

$$\Gamma^{\beta\beta\beta}_{123} = \sum_\lambda\big[F_{1\lambda}\Gamma^{\beta}_{1\lambda}\Gamma^{\beta\beta}_{2,3,\lambda} + (1\leftrightarrow 2) + (1\leftrightarrow 3)\big], \quad (4.9c)$$

$$\Gamma^{\bar\beta\bar\beta\bar\beta}_{123} = \sum_\lambda\big[F_{1\lambda}\Gamma^{\bar\beta}_{-1\lambda}\Gamma^{\bar\beta\bar\beta}_{-2,-3,\lambda} + (1\leftrightarrow 2) + (1\leftrightarrow 3)\big]. \quad (4.9d)$$

Finally, the quartic magnon-magnon interaction is generated from the square of the cubic magnetoelastic coupling via the exchange of a virtual phonon,

$$S_4[\bar\beta,\beta] = -\frac{1}{TN}\sum_{K_1\ldots K_4}\delta_{K_1+\cdots+K_4,0}\Big[\frac{1}{(2!)^2}\Gamma^{\bar\beta\bar\beta\beta\beta}_{12;34}\bar\beta_{-1}\bar\beta_{-2}\beta_3\beta_4 + \frac{1}{3!}\Gamma^{\bar\beta\beta\beta\beta}_{1;234}\bar\beta_{-1}\beta_2\beta_3\beta_4 + \frac{1}{3!}\Gamma^{\bar\beta\bar\beta\bar\beta\beta}_{123;4}\bar\beta_{-1}\bar\beta_{-2}\bar\beta_{-3}\beta_4 + \frac{1}{4!}\Gamma^{\beta\beta\beta\beta}_{1234}\beta_1\beta_2\beta_3\beta_4 + \frac{1}{4!}\Gamma^{\bar\beta\bar\beta\bar\beta\bar\beta}_{1234}\bar\beta_{-1}\bar\beta_{-2}\bar\beta_{-3}\bar\beta_{-4}\Big]. \quad (4.10)$$

The symmetrized quartic vertices are

$$\Gamma^{\bar\beta\bar\beta\beta\beta}_{12;34} = \sum_\lambda\big[F_{1+2,\lambda}\Gamma^{\bar\beta\bar\beta}_{-1,-2,\lambda}\Gamma^{\beta\beta}_{3,4,\lambda} + F_{2+3,\lambda}\Gamma^{\bar\beta\beta}_{-2,3,\lambda}\Gamma^{\bar\beta\beta}_{-1,4,\lambda} + F_{3+1,\lambda}\Gamma^{\bar\beta\beta}_{-1,3,\lambda}\Gamma^{\bar\beta\beta}_{-2,4,\lambda}\big], \quad (4.11a)$$

$$\Gamma^{\bar\beta\beta\beta\beta}_{1;234} = \sum_\lambda\big[F_{1+2,\lambda}\Gamma^{\bar\beta\beta}_{-1,2,\lambda}\Gamma^{\beta\beta}_{3,4,\lambda} + (2\leftrightarrow 3) + (2\leftrightarrow 4)\big], \quad (4.11b)$$

$$\Gamma^{\bar\beta\bar\beta\bar\beta\beta}_{123;4} = \sum_\lambda\big[F_{1+2,\lambda}\Gamma^{\bar\beta\bar\beta}_{-1,-2,\lambda}\Gamma^{\bar\beta\beta}_{-3,4,\lambda} + (2\leftrightarrow 3) + (1\leftrightarrow 3)\big], \quad (4.11c)$$

$$\Gamma^{\beta\beta\beta\beta}_{1234} = \sum_\lambda\big[F_{1+2,\lambda}\Gamma^{\beta\beta}_{1,2,\lambda}\Gamma^{\beta\beta}_{3,4,\lambda} + (2\leftrightarrow 3) + (2\leftrightarrow 4)\big], \quad (4.11d)$$

$$\Gamma^{\bar\beta\bar\beta\bar\beta\bar\beta}_{1234} = \sum_\lambda\big[F_{1+2,\lambda}\Gamma^{\bar\beta\bar\beta}_{-1,-2,\lambda}\Gamma^{\bar\beta\bar\beta}_{-3,-4,\lambda} + (2\leftrightarrow 3) + (2\leftrightarrow 4)\big]. \quad (4.11e)$$

To leading order in $1/S$, the damping of the magnons is determined by the $1/S^2$ correction to the normal component of the magnon self-energy, which can be written as

$$\Sigma_2(K) = \frac{T}{N}\sum_{K'}\Gamma^{\bar\beta\bar\beta\beta\beta}_{-K,-K',K',K}G_0(K') = \frac{T}{N}\sum_{K'\lambda}\big[|\Gamma^{\bar\beta\beta}_{\boldsymbol k,\boldsymbol k',\lambda}|^2 F_0(K-K',\lambda) + |\Gamma^{\beta\beta}_{\boldsymbol k,\boldsymbol k',\lambda}|^2 F_0(K+K',\lambda)\big]G_0(K'), \quad (4.12)$$

where

$$G_0(K) = \frac{1}{i\omega - E_{\boldsymbol k}} \quad (4.13)$$

is the noninteracting magnon Green function.

B. Magnon spectral function and dynamic structure factor

Due to the off-diagonal self-energy $\Pi(K)$ generated by the magnon-phonon interaction, the magnon Green function has also an off-diagonal component, so that we should consider the normal and anomalous propagators. In terms of the normal irreducible self-energies the normal magnon propagator can be written as

$$G(K) = -T\langle\beta_K\bar\beta_K\rangle = -\frac{i\omega + E_{\boldsymbol k} + \Sigma(-K)}{D(K)}, \quad (4.14)$$

while the anomalous magnon propagator is

$$P(K) = -T\langle \beta_K \beta_{-K}\rangle = \frac{\Pi^*(K)}{D(K)}. \tag{4.15}$$

Here

$$D(K) = -[i\omega - \Sigma_-(K)]^2 + [E_{\boldsymbol{k}} + \Sigma_+(K)]^2 - |\Pi(K)|^2 \tag{4.16}$$

can be identified with the determinant of the inverse matrix Green function, and

$$\Sigma_\pm(K) = \tfrac{1}{2}[\Sigma(K) \pm \Sigma(-K)]. \tag{4.17}$$

The spectrum of the magnetoelastic modes can be obtained from the roots of the equation

$$D(\boldsymbol{k},\omega + i\eta) = 0, \tag{4.18}$$

with infinitesimal positive η. Hence, the magnetoelastic modes are determined by

$$\begin{aligned}&[\omega - \Sigma_-(\boldsymbol{k},\omega)]^2 - E_{\boldsymbol{k}}^2 - 2E_{\boldsymbol{k}}\Sigma_+(\boldsymbol{k},\omega)\\ &\quad = [\Sigma_+(\boldsymbol{k},\omega)]^2 - |\Pi(\boldsymbol{k},\omega)|^2.\end{aligned} \tag{4.19}$$

For large effective spin S we may approximate the self-energies by the first order corrections given in Eqs. (4.5) and (4.6). Using the explicit polarization basis given in Eqs. (3.14a)–(3.14c) it is easy to see that $\Sigma_-(K) = 0$ in this approximation, so that we may identify $\Sigma_+(K) = \Sigma(K)$. Still, Eq. (4.19) amounts in general to finding the solutions of a sixth order polynomial. However, the last two terms on the right-hand side involving the square of the self-energies are of order $1/S^2$ and can be neglected; we have checked numerically that these terms do not have any significant effect for the parameters relevant to YIG. The equation for the magnetoelastic modes then reduces to

$$\omega^2 - E_{\boldsymbol{k}}^2 = 2E_{\boldsymbol{k}}\Sigma_1(\boldsymbol{k},\omega), \tag{4.20}$$

where $\Sigma_1(\boldsymbol{k},\omega)$ is defined in Eq. (4.5). To further simplify this equation let us assume that either the energy of the longitudinal phonon mode or the energy of the transverse phonon modes is close to the magnon energy $E_{\boldsymbol{k}}$. In the first case we may approximate

$$\Sigma_1(\boldsymbol{k},\omega) \approx \frac{\left|\Gamma^\beta_{\boldsymbol{k}\parallel}\right|^2}{m\left(\omega^2 - \omega^2_{\boldsymbol{k}\parallel}\right)}, \tag{4.21}$$

while in the second case

$$\Sigma_1(\boldsymbol{k},\omega) \approx \frac{\left|\Gamma^\beta_{\boldsymbol{k}\perp}\right|^2}{m\left(\omega^2 - \omega^2_{\boldsymbol{k}\perp}\right)}, \tag{4.22}$$

where

$$\left|\Gamma^\beta_{\boldsymbol{k}\perp}\right|^2 = \left|\Gamma^\beta_{\boldsymbol{k}\perp,1}\right|^2 + \left|\Gamma^\beta_{\boldsymbol{k}\perp,2}\right|^2. \tag{4.23}$$

Equation (4.20) is then biquadratic and has the solutions

$$\Omega^2_{\boldsymbol{k}\lambda\pm} = \frac{\omega^2_{\boldsymbol{k}\lambda} + E_{\boldsymbol{k}}^2}{2} \pm \sqrt{\frac{\left(\omega^2_{\boldsymbol{k}\lambda} - E_{\boldsymbol{k}}^2\right)^2}{4} + \Delta^4_{\boldsymbol{k}\lambda}}, \tag{4.24}$$

where

$$\Delta^4_{\boldsymbol{k}\lambda} = 2\frac{E_{\boldsymbol{k}}}{m}\left|\Gamma^\beta_{\boldsymbol{k}\lambda}\right|^2. \tag{4.25}$$

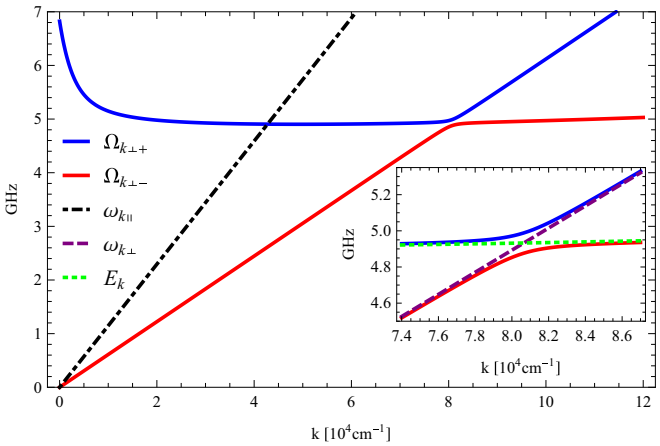

FIG. 2. (Color online) Dispersions of the magnetoelastic modes of a thin YIG stripe with thickness $d = 6.7\,\mu$m in an external magnetic field $H = 1710$ Oe, for $\boldsymbol{k} = k\boldsymbol{e}_z$ parallel to the in-plane magnetic field. The inset shows a magnified view of the hybridization at the crossing of magnon and transverse phonon dispersions.

The energy dispersion of these modes is shown graphically in Fig. 2 for $\boldsymbol{k} = k\boldsymbol{e}_z$ parallel to the in-plane magnetic field. Note that for this propagation direction the longitudinal phonon does not hybridize with the magnon dispersion because for $k_y = 0$ (corresponding to $\theta_{\boldsymbol{k}} = 0$) the relevant hybridization function $\Gamma_{\boldsymbol{k}\parallel}$ given in Eq. (3.29a) vanishes.

The normal component of the magnon Green function is in this approximation

$$G(\boldsymbol{k},i\omega) = \frac{i\omega + E_{\boldsymbol{k}} + \Sigma_1(\boldsymbol{k},i\omega)}{(i\omega)^2 - E_{\boldsymbol{k}}^2 - 2E_{\boldsymbol{k}}\Sigma_1(\boldsymbol{k},i\omega)}. \tag{4.26}$$

If $i\omega$ is close to $\omega_{\boldsymbol{k}\lambda}$ this can be approximated by

$$G(\boldsymbol{k},i\omega) \approx \frac{[i\omega + E_{\boldsymbol{k}}]\left[(i\omega)^2 - \omega^2_{\boldsymbol{k}\lambda}\right] + \frac{|\Gamma^\beta_{\boldsymbol{k}\lambda}|^2}{m}}{\left[(i\omega)^2 - E_{\boldsymbol{k}}^2\right]\left[(i\omega)^2 - \omega^2_{\boldsymbol{k}\lambda}\right] - 2E_{\boldsymbol{k}}\frac{|\Gamma^\beta_{\boldsymbol{k}\lambda}|^2}{m}}. \tag{4.27}$$

After analytic continuation to the real frequency axis we obtain for the corresponding spectral function

$$\begin{aligned}A(\boldsymbol{k},\omega) &= -\frac{1}{\pi}\mathrm{Im}G(\boldsymbol{k},\omega + i\eta)\\ &\approx Z_{\boldsymbol{k}\lambda}(\omega)\sum_{s=\pm} s[\delta(\omega - \Omega_{\boldsymbol{k}\lambda s}) + \delta(\omega + \Omega_{\boldsymbol{k}\lambda s})],\end{aligned} \tag{4.28}$$

where

$$Z_{\boldsymbol{k}\lambda}(\omega) = \frac{[\omega + E_{\boldsymbol{k}}]\left[\omega^2 - \omega^2_{\boldsymbol{k}\lambda}\right] + \frac{|\Gamma^\beta_{\boldsymbol{k}\lambda}|^2}{m}}{2\omega\left[\Omega^2_{\boldsymbol{k}\lambda+} - \Omega^2_{\boldsymbol{k}\lambda-}\right]}. \tag{4.29}$$

An intensity plot of the magnon spectral function for YIG is shown in Fig. 3. One clearly sees the transfer of spectral weight between the magnon and the phonon branch at the crossing point. Actually, the Brillouin light scattering intensity is proportional to the transverse spin structure

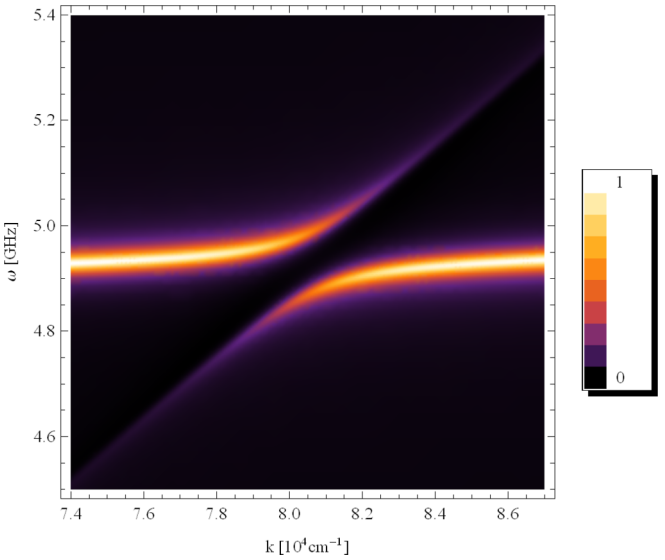

FIG. 3. (Color online) Magnon spectral function $A(\boldsymbol{k},\omega)$ of a thin YIG stripe with thickness $d = 6.7\,\mu$m in an external magnetic field $H = 1710$ Oe, for $\boldsymbol{k} = k\boldsymbol{e}_z$ parallel to the in-plane magnetic field. The Dirac distributions were artificially broadened with a lifetime of 10 ns.

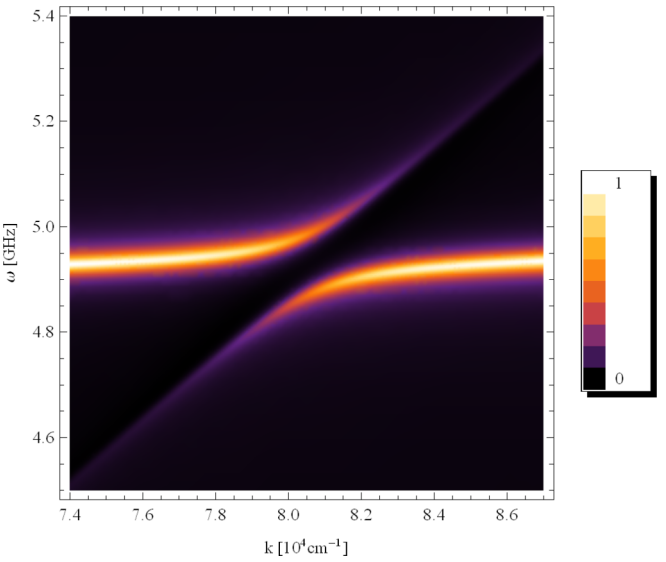

FIG. 4. (Color online) Transverse spin dynamic structure factor of a thin YIG stripe at temperature $T = 300$ K, with thickness $d = 6.7\,\mu$m in an external magnetic field $H = 1710$ Oe, for $\boldsymbol{k} = k\boldsymbol{e}_z$ parallel to the in-plane magnetic field. The Dirac distributions were artificially broadened with a lifetime of 10 ns.

factor [26,27]

$$S_\perp(\boldsymbol{k},\omega) = \int_{-\infty}^{\infty} \frac{dt}{2\pi} e^{i\omega t}\left\langle S^x_{-\boldsymbol{k}}(0)S^x_{\boldsymbol{k}}(t) + S^y_{-\boldsymbol{k}}(0)S^y_{\boldsymbol{k}}(t)\right\rangle, \quad (4.30)$$

where the Fourier transform of the spin operator is defined in Eq. (3.18). To leading order in spin wave theory we obtain

$$S_\perp(\boldsymbol{k},\omega) = \frac{S}{1-e^{-\omega/T}}\left\{\left(u_{\boldsymbol{k}}^2 + |v_{\boldsymbol{k}}|^2\right)[A(-\boldsymbol{k},\omega) - A(\boldsymbol{k},-\omega)] - 2(u_{\boldsymbol{k}}v_{\boldsymbol{k}}^* + u_{\boldsymbol{k}}v_{\boldsymbol{k}})B(\boldsymbol{k},\omega)\right\}, \quad (4.31)$$

where

$$B(\boldsymbol{k},\omega) = -\frac{1}{\pi}\mathrm{Im}P(\boldsymbol{k},\omega + i\eta) \quad (4.32)$$

is the spectral function of the anomalous magnon Green function $P(\boldsymbol{k},i\omega)$, which for imaginary frequencies is defined by Eq. (4.15). We obtain

$$B(\boldsymbol{k},\omega) \approx Y_{\boldsymbol{k}\lambda}(\omega)\sum_{s=\pm} s[\delta(\omega - \Omega_{\boldsymbol{k}\lambda s}) + \delta(\omega + \Omega_{\boldsymbol{k}\lambda s})], \quad (4.33)$$

where

$$Y_{\boldsymbol{k}\lambda}(\omega) = -\frac{\Gamma^{\bar\beta}_{-\boldsymbol{k}\perp,1}\Gamma^{\bar\beta}_{\boldsymbol{k}\perp,1} + \Gamma^{\bar\beta}_{-\boldsymbol{k}\perp,2}\Gamma^{\bar\beta}_{\boldsymbol{k}\perp,2}}{2m\omega\left[\Omega^2_{\boldsymbol{k}\lambda+} - \Omega^2_{\boldsymbol{k}\lambda-}\right]}. \quad (4.34)$$

An intensity plot of the transverse dynamic structure factor is shown in Fig. 4. Note that the qualitative behavior is very similar to the behavior of the magnon spectral function, which is due to the fact that the Bogoliubov transformation has only a small effect because of the smallness of the Boguliubov coefficient $v_{\boldsymbol{k}}$ in the entire Brillouin zone.

V. MAGNON DAMPING

In this section we calculate the decay rate (i.e., the damping) of the magnons due to the magnon-phonon interaction in YIG at room temperature. The damping $\gamma(\boldsymbol{k})$ of magnons with wave vector $\boldsymbol{k}$ and energy $E_{\boldsymbol{k}}$ can be obtained from the imaginary part of the self-energy $\Sigma(K) = \Sigma(\boldsymbol{k},i\omega)$ after analytic continuation to the real frequency axis,

$$\gamma(\boldsymbol{k}) = -\mathrm{Im}\Sigma(\boldsymbol{k},i\omega \to E_{\boldsymbol{k}} + i\eta). \quad (5.1)$$

To leading order in $1/S$ the damping is determined by the second order self-energy given in Eq. (4.12); after carrying out the frequency sum we obtain

$$\Sigma_2(\boldsymbol{k},i\omega) = \frac{1}{N}\sum_{\boldsymbol{k}'\lambda}\left\{\frac{\left|\Gamma^{\bar\beta\beta}_{\boldsymbol{k},\boldsymbol{k}',\lambda}\right|^2}{2m\omega_{\boldsymbol{k}-\boldsymbol{k}'\lambda}}\left[\frac{b(\omega_{\boldsymbol{k}-\boldsymbol{k}'\lambda}) - b(E_{\boldsymbol{k}'})}{i\omega + \omega_{\boldsymbol{k}-\boldsymbol{k}'\lambda} - E_{\boldsymbol{k}'}} + \frac{1 + b(\omega_{\boldsymbol{k}-\boldsymbol{k}'\lambda}) + b(E_{\boldsymbol{k}'})}{i\omega - \omega_{\boldsymbol{k}-\boldsymbol{k}'\lambda} - E_{\boldsymbol{k}'}}\right] - \frac{\left|\Gamma^{\beta\beta}_{\boldsymbol{k},\boldsymbol{k}',\lambda}\right|^2}{2m\omega_{\boldsymbol{k}+\boldsymbol{k}'\lambda}}\left[\frac{1 + b(\omega_{\boldsymbol{k}+\boldsymbol{k}'\lambda}) + b(E_{\boldsymbol{k}'})}{i\omega + \omega_{\boldsymbol{k}+\boldsymbol{k}'\lambda} + E_{\boldsymbol{k}'}} + \frac{b(\omega_{\boldsymbol{k}+\boldsymbol{k}'\lambda}) - b(E_{\boldsymbol{k}'})}{i\omega - \omega_{\boldsymbol{k}+\boldsymbol{k}'\lambda} + E_{\boldsymbol{k}'}}\right]\right\}. \quad (5.2)$$

Here $b(\omega) = 1/(e^{\omega/T} - 1)$ is the Bose function. The corresponding damping function off resonance is

$$\gamma_2(\boldsymbol{k},\omega) = -\mathrm{Im}\Sigma_2(\boldsymbol{k},\omega + i\eta) = (1 - e^{-\omega/T})\frac{\pi}{N}\sum_{\boldsymbol{k}'\lambda}\left(\frac{\left|\Gamma^{\bar{\beta}\beta}_{\boldsymbol{k},\boldsymbol{k}',\lambda}\right|^2}{2m\omega_{\boldsymbol{k}-\boldsymbol{k}'\lambda}}\{\delta(\omega - E_{\boldsymbol{k}'} + \omega_{\boldsymbol{k}-\boldsymbol{k}'\lambda})[1 + b(E_{\boldsymbol{k}'})]b(\omega_{\boldsymbol{k}-\boldsymbol{k}'\lambda})\right.$$
$$+ \delta(\omega - E_{\boldsymbol{k}'} - \omega_{\boldsymbol{k}-\boldsymbol{k}'\lambda})[1 + b(E_{\boldsymbol{k}'})][1 + b(\omega_{\boldsymbol{k}-\boldsymbol{k}'\lambda})]\} + \frac{\left|\Gamma^{\beta\beta}_{\boldsymbol{k},\boldsymbol{k}',\lambda}\right|^2}{2m\omega_{\boldsymbol{k}+\boldsymbol{k}'\lambda}}\{\delta(\omega + E_{\boldsymbol{k}'} + \omega_{\boldsymbol{k}+\boldsymbol{k}'\lambda})b(E_{\boldsymbol{k}'})b(\omega_{\boldsymbol{k}+\boldsymbol{k}'\lambda})$$
$$\left. + \delta(\omega + E_{\boldsymbol{k}'} - \omega_{\boldsymbol{k}-\boldsymbol{k}'\lambda})b(E_{\boldsymbol{k}'})[1 + b(\omega_{\boldsymbol{k}+\boldsymbol{k}'\lambda})]\}\right). \tag{5.3}$$

Since the experiments of interest to us are performed at room temperature, which is large compared with all other energy scales, we may use the high-temperature expansion of the Bose functions, $b(\omega) \approx T/\omega$. Setting now $\omega = E_{\boldsymbol{k}}$ we obtain for the magnon damping on resonance at high temperatures,

$$\gamma_2(\boldsymbol{k}) = \frac{\pi T E_{\boldsymbol{k}}}{2mN}\sum_{\boldsymbol{k}'\lambda}\left\{\frac{\left|\Gamma^{\bar{\beta}\beta}_{\boldsymbol{k},\boldsymbol{k}',\lambda}\right|^2}{E_{\boldsymbol{k}'}\omega^2_{\boldsymbol{k}-\boldsymbol{k}'\lambda}}[\delta(E_{\boldsymbol{k}} - E_{\boldsymbol{k}'} + \omega_{\boldsymbol{k}-\boldsymbol{k}'\lambda}) + \delta(E_{\boldsymbol{k}} - E_{\boldsymbol{k}'} - \omega_{\boldsymbol{k}-\boldsymbol{k}'\lambda})] + \frac{\left|\Gamma^{\beta\beta}_{\boldsymbol{k},\boldsymbol{k}',\lambda}\right|^2}{E_{\boldsymbol{k}'}\omega^2_{\boldsymbol{k}+\boldsymbol{k}'\lambda}}\delta(E_{\boldsymbol{k}} + E_{\boldsymbol{k}'} - \omega_{\boldsymbol{k}+\boldsymbol{k}'\lambda})\right\}$$
$$= \gamma^{\mathrm{Che}}_{2a}(\boldsymbol{k}) + \gamma^{\mathrm{Che}}_{2b}(\boldsymbol{k}) + \gamma^{\mathrm{con}}_{2}(\boldsymbol{k}), \tag{5.4}$$

where

$$\gamma^{\mathrm{Che}}_{2a}(\boldsymbol{k}) = \frac{\pi T E_{\boldsymbol{k}}}{2mN}\sum_{\boldsymbol{q}\lambda}\frac{\left|\Gamma^{\bar{\beta}\beta}_{\boldsymbol{k},\boldsymbol{k}+\boldsymbol{q},\lambda}\right|^2}{E_{\boldsymbol{k}+\boldsymbol{q}}\omega^2_{\boldsymbol{q}\lambda}}\delta(E_{\boldsymbol{k}} - E_{\boldsymbol{k}+\boldsymbol{q}} + \omega_{\boldsymbol{q}\lambda}), \tag{5.5}$$

$$\gamma^{\mathrm{Che}}_{2b}(\boldsymbol{k}) = \frac{\pi T E_{\boldsymbol{k}}}{2mN}\sum_{\boldsymbol{q}\lambda}\frac{\left|\Gamma^{\bar{\beta}\beta}_{\boldsymbol{k},\boldsymbol{k}-\boldsymbol{q},\lambda}\right|^2}{E_{\boldsymbol{k}-\boldsymbol{q}}\omega^2_{\boldsymbol{q}\lambda}}\delta(E_{\boldsymbol{k}} - E_{\boldsymbol{k}-\boldsymbol{q}} - \omega_{\boldsymbol{q}\lambda}), \tag{5.6}$$

$$\gamma^{\mathrm{con}}_{2}(\boldsymbol{k}) = \frac{\pi T E_{\boldsymbol{k}}}{2mN}\sum_{\boldsymbol{q}\lambda}\frac{\left|\Gamma^{\beta\beta}_{\boldsymbol{k},-\boldsymbol{k}+\boldsymbol{q},\lambda}\right|^2}{E_{-\boldsymbol{k}+\boldsymbol{q}}\omega^2_{\boldsymbol{q}\lambda}}\delta(E_{\boldsymbol{k}} + E_{-\boldsymbol{k}+\boldsymbol{q}} - \omega_{\boldsymbol{q}\lambda}). \tag{5.7}$$

The contributions $\gamma^{\mathrm{Che}}_{2a}(\boldsymbol{k})$ and $\gamma^{\mathrm{Che}}_{2b}(\boldsymbol{k})$ are due to the Cherenkov type process where a magnon with energy $E_{\boldsymbol{k}}$ emits or absorbs a phonon with energy $\omega_{\boldsymbol{q}}$ and decays into a magnon with energy $E_{\boldsymbol{k}\pm\boldsymbol{q}}$. The last contribution $\gamma^{\mathrm{con}}_{2}(\boldsymbol{k})$ describes a confluent scattering process where two magnons with energies $E_{\boldsymbol{k}}$ and $E_{-\boldsymbol{k}+\boldsymbol{q}}$ decay into a phonon with energy $\omega_{\boldsymbol{q}}$. The corresponding Feynman diagrams are shown in Fig. 5. Taking into account that for YIG the interaction vertices in the quasiparticle basis can be approximated by the corresponding interaction vertices in the Holstein-Primakoff basis, we may approximate the squared matrix elements in the above expressions by

$$\left|\Gamma^{\bar{\beta}\beta}_{\boldsymbol{k},\boldsymbol{k}\pm\boldsymbol{q},\lambda}\right|^2 \equiv \left|\boldsymbol{e}^*_{\boldsymbol{q}\lambda}\cdot\boldsymbol{\Gamma}^{\bar{\beta}\beta}_{\boldsymbol{k},\boldsymbol{k}\pm\boldsymbol{q}}\right|^2 \approx \left|\boldsymbol{e}^*_{\boldsymbol{q}\lambda}\cdot\boldsymbol{\Gamma}^{\bar{b}b}_{\boldsymbol{k},\boldsymbol{k}\pm\boldsymbol{q}}\right|^2$$
$$= |\boldsymbol{e}^*_{\boldsymbol{q}\lambda}\cdot\boldsymbol{U}_{\pm\boldsymbol{q}}|^2 \equiv |\boldsymbol{q}|^2U^2_\lambda(\hat{\boldsymbol{q}}), \tag{5.8}$$

$$\left|\Gamma^{\beta\beta}_{\boldsymbol{k},-\boldsymbol{k}+\boldsymbol{q},\lambda}\right|^2 \equiv \left|\boldsymbol{e}^*_{\boldsymbol{q}\lambda}\cdot\boldsymbol{\Gamma}^{\beta\beta}_{\boldsymbol{k},-\boldsymbol{k}+\boldsymbol{q}}\right|^2 \approx \left|\boldsymbol{e}^*_{\boldsymbol{q}\lambda}\cdot\boldsymbol{\Gamma}^{bb}_{\boldsymbol{k},-\boldsymbol{k}+\boldsymbol{q}}\right|^2$$
$$= |\boldsymbol{e}^*_{\boldsymbol{q}\lambda}\cdot\boldsymbol{V}_{\boldsymbol{q}}|^2 \equiv |\boldsymbol{q}|^2V^2_\lambda(\hat{\boldsymbol{q}}), \tag{5.9}$$

where

$$U^2_\lambda(\hat{\boldsymbol{q}}) = \frac{B^2_\parallel}{S^2}|\boldsymbol{e}^*_{\boldsymbol{q}\lambda}\cdot(\hat{q}_x\boldsymbol{e}_y + \hat{q}_y\boldsymbol{e}_x - 2\hat{q}_z\boldsymbol{e}_z)|^2, \tag{5.10}$$

$$V^2_\lambda(\hat{\boldsymbol{q}}) = \frac{B^2_\parallel}{S^2}|\boldsymbol{e}^*_{\boldsymbol{q}\lambda}\cdot(\hat{q}_x\boldsymbol{e}_x - \hat{q}_y\boldsymbol{e}_y)|^2$$
$$+ \frac{B^2_\perp}{S^2}|\boldsymbol{e}^*_{\boldsymbol{q}\lambda}\cdot(\hat{q}_x\boldsymbol{e}_y + \hat{q}_y\boldsymbol{e}_x)|^2. \tag{5.11}$$

Here $\hat{q}_\alpha = q_\alpha/|\boldsymbol{q}|$ are the components of the unit vector in the direction of $\boldsymbol{q}$. Using the phonon basis in Eqs. (3.14a)–(3.14c) we obtain for $q_x = 0$,

$$U^2_\parallel(\hat{\boldsymbol{q}}) = \frac{B^2_\parallel}{S^2}\left(\hat{q}^2_y - 2\hat{q}^2_z\right)^2 = \frac{B^2_\parallel}{S^2}(1 - 3\cos^2\theta_{\boldsymbol{q}})^2, \tag{5.12a}$$

$$U^2_{\perp 1}(\hat{\boldsymbol{q}}) = \frac{B^2_\parallel}{S^2}(3\hat{q}_y\hat{q}_z)^2 = \frac{B^2_\parallel}{S^2}\frac{9}{4}\sin^2(2\theta_{\boldsymbol{q}}), \tag{5.12b}$$

$$U^2_{\perp 2}(\hat{\boldsymbol{q}}) = 0, \tag{5.12c}$$

and

$$V^2_\parallel(\hat{\boldsymbol{q}}) = \frac{B^2_\parallel}{S^2}\hat{q}^4_y = \frac{B^2_\parallel}{S^2}\sin^4\theta_{\boldsymbol{q}}, \tag{5.13a}$$

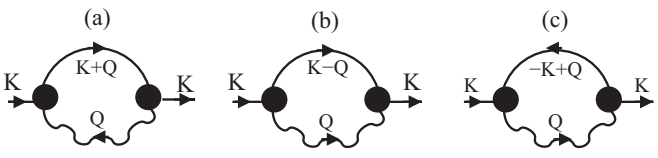

FIG. 5. These Feynman diagrams gives rise to the three contributions to the magnon decay rate given in Eqs. (5.5)–(5.7): (a) Cherenkov process with absorption of a virtual phonon, (b) Cherenkov process with emission of a virtual phonon, and (c) confluent process. The solid arrows represent magnon propagators while the wavy arrows represent phonon propagators. The arrows represent the direction of the energy-momentum flow. Black dots represent the relevant components of the three-legged vertices $\boldsymbol{\Gamma}^{\bar{\beta}\beta}$ and $\boldsymbol{\Gamma}^{\beta\beta}$ defined in Eqs. (3.37a) and (3.37b).

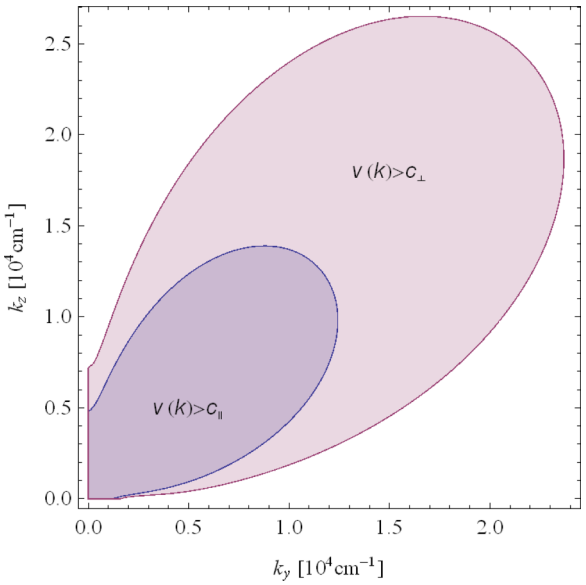

FIG. 6. (Color online) The shaded areas denote the momentum range where the group velocity $v(\boldsymbol{k})$ of the magnons exceeds either the longitudinal or the transverse phonon velocity. The parameters are the same as in Fig. 4.

$$V_{\perp 1}^2(\hat{\boldsymbol{q}}) = \frac{B_\parallel^2}{S^2}(\hat{q}_y\hat{q}_z)^2 = \frac{B_\parallel^2}{S^2}\frac{1}{4}\sin^2(2\theta_{\boldsymbol{q}}), \tag{5.13b}$$

$$V_{\perp 2}^2(\hat{\boldsymbol{q}}) = \frac{B_\perp^2}{S^2}\hat{q}_y^2 = \frac{B_\perp^2}{S^2}\sin^2\theta_{\boldsymbol{q}}, \tag{5.13c}$$

where we have set $\hat{q}_z = \cos\theta_{\boldsymbol{q}}$ and $\hat{q}_y = \sin\theta_{\boldsymbol{q}}$.

A. Dipolar regime: Theory

In the long-wavelength regime $|\boldsymbol{k}| \lesssim \sqrt{\Delta/\rho_s}$ the behavior of the magnon damping (5.4) strongly depends on the size $v(\boldsymbol{k}) = |\boldsymbol{v}(\boldsymbol{k})|$ of the group velocity $\boldsymbol{v}(\boldsymbol{k}) = \nabla_{\boldsymbol{k}} E_{\boldsymbol{k}}$ of the magnons in comparison with the phonon velocities. In Fig. 6 we show the momentum range where the magnon velocity $v(\boldsymbol{k})$ exceeds the phonon velocities c_λ. In regime around the minima of the dispersion, the velocity $v(\boldsymbol{k})$ is small compared with the phonon velocities, while at very small wave vectors $v(\boldsymbol{k}) > c_\lambda$. In this regime around the minima of the dispersion the decay rate of the magnons is dominated by the confluent process given in Eq. (5.7) because the Cherenkov processes are kinematically suppressed. In fact, in a substantial regime around dispersion minima the quasiparticle velocity is small compared with the phonon velocities, so that we may approximate $E_{-\boldsymbol{k}+\boldsymbol{q}} \approx E_{\boldsymbol{k}} - \boldsymbol{v}(\boldsymbol{k})\cdot\boldsymbol{q}$ and expand the decay rate in powers of $v(\boldsymbol{k})/c_\lambda$. The momentum integration in Eq. (5.7) can then be carried out and we obtain

$$\gamma_2^{\text{con}}(\boldsymbol{k}) = \frac{T}{4S^2}\frac{E_{\boldsymbol{k}}}{m}\frac{a^2}{}\left[\frac{B_\perp^2}{c_\perp^4}\left(1+\frac{3}{4}\frac{v_y^2(\boldsymbol{k})}{c_\perp^2}+\frac{v_z^2(\boldsymbol{k})}{4c_\perp^2}\right)\right.$$
$$+\frac{B_\parallel^2}{4c_\perp^4}\left(1+\frac{v_y^2(\boldsymbol{k})}{2c_\perp^2}+\frac{v_z^2(\boldsymbol{k})}{2c_\perp^2}\right)$$
$$\left.+\frac{3}{4}\frac{B_\parallel^2}{c_\parallel^4}\left(1+\frac{5}{6}\frac{v_y^2(\boldsymbol{k})}{c_\parallel^2}+\frac{v_z^2(\boldsymbol{k})}{6c_\parallel^2}\right)\right]. \tag{5.14}$$

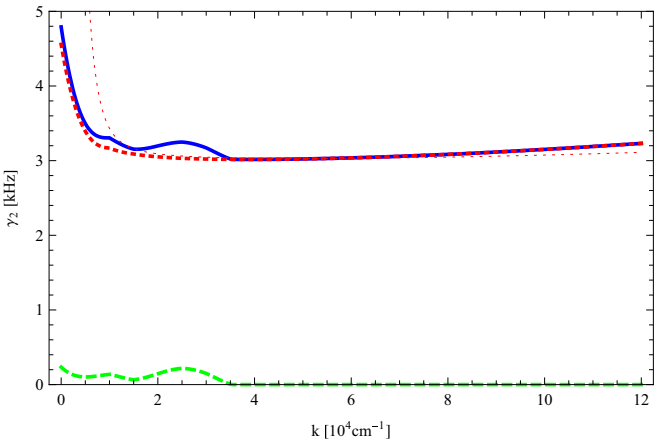

FIG. 7. (Color online) Numerical evaluation of our result (5.4) for the damping rate of magnons in a thin YIG stripe at temperature $T = 300$ K, in the dipolar momentum regime. The plot is for a thin stripe of thickness $d = 6.7\ \mu$m in an external magnetic field $H = 1710$ Oe, for $\boldsymbol{k} = k\boldsymbol{e}_z$ parallel to the in-plane magnetic field. Solid lines correspond to the total damping rate, while the dashed and the dotted lines are the contribution from the Cherenkov and the confluent processes, respectively. The corresponding thin dotted line is the approximation (5.14) in the dipolar momentum regime.

The confluent contribution to the high-temperature damping rate in the dipolar regime is shown graphically as the thin dotted line in Fig. 7. On the other hand, the Cherenkov-type process contributes only for very small $\boldsymbol{k}$, when $v(\boldsymbol{k}) \gtrsim c_\lambda$, see Fig. 6. However, for those momenta it is no longer valid to linearize the dispersion due to the strong effect of the Bogoliubov transformation, and no analytical approximation can be obtained. Therefore we only present the numerical solution as dashed line in Fig. 7. Obviously, apart from an enhancement for $k \lesssim 2\times10^4\ \text{cm}^{-1}$, the damping exhibits a rather weak dependence on the wave vector in this regime.

B. Dipolar regime: Experiment

For a comparison of our calculation with experiments one should keep in mind that we have only considered the contribution from the magnon-phonon interactions on the damping of the magnons. Of course, in the real system there are other sources leading to magnon decay, such as magnon-magnon interactions or the elastic scattering of magnons by impurities. We therefore expect that the magnon damping due to magnon-phonon interactions is a lower limit to the experimentally observed magnon damping rate. In fact, our experimental data presented below show that in the dipolar regime magnon-phonon interactions are not the dominant source of magnon damping.

In order to determine the relaxation time of different groups of magnons, a measurements of the spectral distribution of magnon gas densities as a function of the frequency and wave vector using time- and wave-vector-resolved BLS spectroscopy [14] has been performed. Due to technical reasons only in-plane wave vectors from 0 up to the $k_z^{\max} = 11\times10^4\ \text{cm}^{-1}$ are accessible within our apparatus. The measurements were performed using a YIG film with thickness

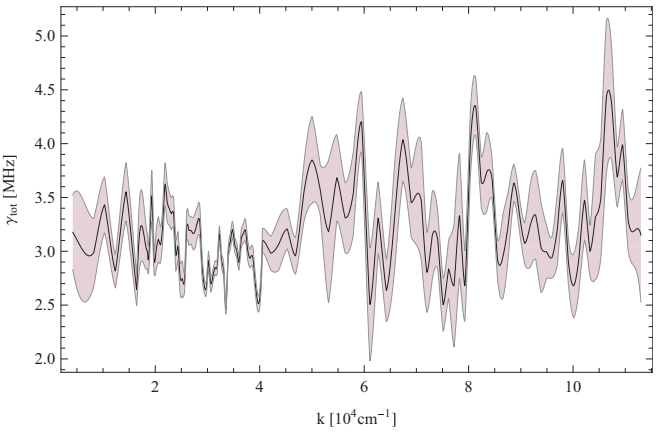

FIG. 8. (Color online) Experimentally determined dependence of the total magnon damping $\gamma_{\rm tot}$ on the in-plane wave vector in the dipolar regime where the magnon dispersion is dominated by the competition between the dipole-dipole and the exchange interaction. The shaded regions represent the estimated experimental uncertainties.

6.7 μm, which was liquid-phase epitaxialy grown on a 500 μm thick gallium gadolinium garnet substrate.

The magnon spectrum was populated by intensive thermalization [25,28,29] of magnons, which were injected by the parallel parametric pumping technique [30] at half of the pumping frequency $f_p = 13.62$ GHz. The bias magnetic field of $H = 1710$ Oe was tuned to provide the excitation of parametric magnons at the ferromagnetic resonance frequency. In this case the direct transition of magnons to the bottom of spin wave spectrum is prohibited by conservation laws. This ensures high efficiency of multistage four-magnon scattering which is necessary for thermalization and thus population of the spectrum.

We have measured the redistribution of thermalized magnons along the fundamental backward-volume magnetostatic spin wave mode as a function of time and wave vector. After switching off the pumping, the magnons are allowed to relax freely. By fitting the relaxation times for different groups of thermalized magnons we were able to extract the damping rates. The obtained dependence of measured total damping rate $\gamma_{\rm tot}$ on the in-plane wave vector for dipolar-exchange spin waves is shown in Fig. 8. Obviously the value of relaxation rate is roughly three orders of magnitude larger than our calculated relaxation rate due to magnon-phonon interactions shown Fig. 7. We thus conclude that in the long-wavelength dipolar regime other relaxation channels (in particular two-magnon scattering processes [31–34]) dominate the magnon damping. The rather irregular behavior of the measured damping rate in Fig. 8 suggests that elastic scattering of magnons by impurities might play an important role in this regime. Note that within the tolerance limits of the experiment the measured relaxation rate has a rather weak dependence on the in-plane wave vectors in the entire accessible range of wave vectors. In this respect the experimental results agree with our prediction of a momentum-independent damping rate in this regime.

Unfortunately, microscopic calculations of the magnon decay rates at room temperature, taking magnon-impurity and magnon-magnon interactions into account, are not available in the momentum range relevant for our experiment. One should keep in mind, however, that magnon-impurity scattering can only explain the momentum relaxation of the magnon gas; for the equilibration of the different temperatures of the magnon and the phonon systems magnon-phonon interactions are essential.

C. Exchange regime

For wave vectors in the regime where the exchange energy $\rho_s k^2$ exceeds the characteristic dipolar energy Δ we may ignore the dipole-dipole interaction in the magnon dispersion (2.11) and approximate the long-wavelength magnon dispersion by $E_{\boldsymbol{k}} \approx h + \rho_s \boldsymbol{k}^2$. Then the evaluation of the integrals in Eqs. (5.5)–(5.7) simplifies. We obtain for the Cherenkov part

$$\gamma_2^{\rm Che}(\boldsymbol{k}) \equiv \gamma_{2a}^{\rm Che}(\boldsymbol{k}) + \gamma_{2b}^{\rm Che}(\boldsymbol{k}) = \frac{T E_{\boldsymbol{k}}}{2} \frac{m_s}{m} \sum_\lambda \frac{a^2}{c_\lambda^2} \times \int_0^{2\pi} \frac{d\varphi}{2\pi} \frac{U_\lambda^2(\hat{\boldsymbol{q}}_\varphi)}{E_{\boldsymbol{k}} + 2m_s c_\lambda [c_\lambda - v(\boldsymbol{k}) \cos\varphi]}. \tag{5.15}$$

where $v(\boldsymbol{k}) = |\boldsymbol{k}|/m_s$, the mass m_s is defined via $\rho_s = 1/(2m_s)$, and the angle-dependent unit vector $\hat{\boldsymbol{q}}_\varphi$ is defined by

$$\hat{\boldsymbol{q}}_\varphi = [\hat{v}_y(\boldsymbol{k}) \cos\varphi - \hat{v}_z(\boldsymbol{k}) \sin\varphi] \boldsymbol{e}_y + [\hat{v}_z(\boldsymbol{k}) \cos\varphi + \hat{v}_y(\boldsymbol{k}) \sin\varphi] \boldsymbol{e}_z. \tag{5.16}$$

Here $\hat{v}_\alpha(\boldsymbol{k})$ are the components of the unit vector in the direction of the magnon velocity $\boldsymbol{v}(\boldsymbol{k}) = \nabla_{\boldsymbol{k}} E_{\boldsymbol{k}} = \boldsymbol{k}/m_s$. Although the angular integration in Eq. (5.15) can be done analytically, the result is not very transparent so that we omit it here. A graph of the Cherenkov contribution to the high-temperature damping rate in the exchange regime is shown as the thin dashed line in Fig. 9. Next, consider the contribution (5.7) of the confluent scattering process to the damping rate in the exchange regime. Setting again $E_{\boldsymbol{k}} \approx h + \rho_s \boldsymbol{k}^2$ and carrying out the integration over $|\boldsymbol{q}|$ we obtain

$$\gamma_2^{\rm con}(\boldsymbol{k}) = \frac{T E_{\boldsymbol{k}}}{4} \frac{a^2}{m} \sum_\lambda \int_0^{2\pi} \frac{d\varphi}{2\pi} \frac{V_\lambda^2(\hat{\boldsymbol{q}}_\varphi)}{c_\lambda^3} \times \frac{\Theta\left[c_\lambda + v(\boldsymbol{k}) \cos\varphi - \sqrt{\frac{4E_{\boldsymbol{k}}}{m_s}}\right]}{\sqrt{[c_\lambda + v(\boldsymbol{k}) \cos\varphi]^2 - \frac{4E_{\boldsymbol{k}}}{m_s}}} \times \left[\frac{c_\lambda q_+}{c_\lambda q_+ - E_{\boldsymbol{k}}} + \frac{c_\lambda q_-}{c_\lambda q_- - E_{\boldsymbol{k}}}\right], \tag{5.17}$$

where

$$q_\pm = m_s [c_\lambda + v(\boldsymbol{k}) \cos\varphi] \pm m_s \sqrt{[c_\lambda + v(\boldsymbol{k}) \cos\varphi]^2 - \frac{4E_{\boldsymbol{k}}}{m_s}}. \tag{5.18}$$

The confluent contribution to the high-temperature damping rate in the exchange regime is shown graphically as the thin

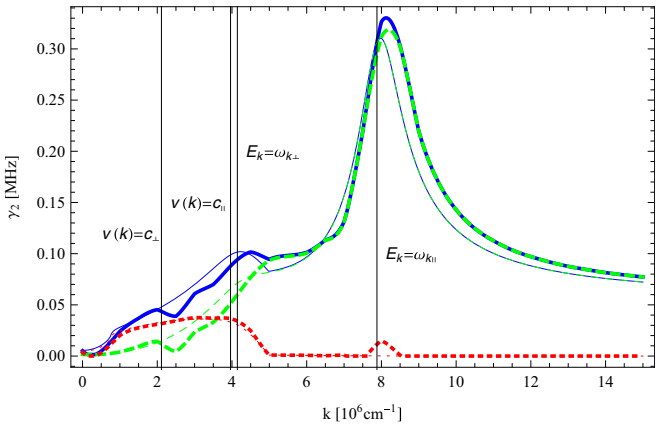

FIG. 9. (Color online) Numerical evaluation of our result (5.4) for the damping rate of magnons in a thin YIG stripe at temperature $T = 300$ K, in the exchange momentum regime. The plot is for a thin stripe of thickness $d = 6.7\,\mu$m in an external magnetic field $H = 1710$ Oe, for $\boldsymbol{k} = k\boldsymbol{e}_z$ parallel to the in-plane magnetic field. Solid lines correspond to the total damping rate, while the dashed and the dotted lines are the contribution from the Cherenkov and the confluent processes, respectively. The corresponding thin lines are the approximations in the exchange momentum regime, see Eqs. (5.15) and (5.17).

dotted line in Fig. 9. As one can see, the magnon damping is strongly $\boldsymbol{k}$ dependent. In particular, it exhibits peaks at the crossing points of magnon and phonon dispersions as well as velocities. It also increases by two orders of magnitude between dipolar and exchange regimes, which are dominated by confluence and Cherenkov processes, respectively. For the magnon lifetime $\tau(\boldsymbol{k}) = 1/[2\pi\gamma(\boldsymbol{k})]$, this implies values of the order of 50 μs in the dipolar momentum range, while it can be as low as 480 ns for exchange momenta.

VI. SUMMARY AND CONCLUSIONS

In this work we have studied magnetoelastic interactions in experimentally relevant thin films of the magnetic insulator YIG. As the dominant sources of magnetoelastic interactions are due to relativistic effects [9], which cannot be taken into account within an effective model containing only spin degrees of freedom, we have used a semiphenomenological approach [2], which relies on the quantization of a suitable phenomenological expression for the magnetoelastic energy. For the quantized theory we have then carefully derived the momentum dependence of the magnetoelastic interaction vertices within the framework of the conventional $1/S$ expansion for ordered quantum spin systems. Using these vertices, we have explicitly calculated the leading contributions to the hybridization between magnon and phonon modes, as well as the damping of the magnons due to spin-lattice coupling. The hybridization has been shown to give rise to a characteristic minimum in the spin dynamic structure factor at the crossing point of magnon and transversal phonon dispersions, where the spectral weight is transferred from the magnons to the transverse phonon mode. The position of this minimum quantitatively agrees with the recent experimental observation of the magnetoelastic mode [35].

The damping at room temperature has been shown to be strongly momentum dependent. In the long-wavelength dipolar regime it is rather flat and almost exclusively driven by confluent magnon-phonon scattering processes where two magnons decay into a phonon or vice versa. In this regime we have also presented experimental results for the magnon damping obtained by wave-vector-resolved Brillouin light scattering spectroscopy. The fact that the experimental results for the magnon damping are roughly three orders of magnitude larger than our theoretical results indicate that in the dipolar regime magnon-phonon interactions are not the dominant source of magnon damping in our samples at room temperature. We suspect that in this regime the magnon damping is dominated by elastic scattering of magnons from impurities. On the other hand, in the short-wavelength exchange regime the damping is due to magnon-phonon scattering processes of the Cherenkov type and is two orders of magnitude larger than in the dipolar regime. The damping rate exhibits pronounced peaks at the crossing points of magnon and phonon dispersions and velocities. This agrees very well with the conclusions of the experiment [12], where the authors suggested that the spin-lattice relaxation in the dipolar regime should be much slower than in the exchange regime in order to reconcile their results with earlier work on the spin Seebeck effect.

The present work can be extended in two directions: On the theoretical side, it would be useful to have quantitatively accurate calculations of the magnon damping due to magnon-impurity and magnon-magnon interactions in the dipolar regime; we expect that this can provide a better explanation for our experimental results shown in Fig. 8, which is three orders of magnitude larger than the damping due to magnon-phonon interactions in this regime. Note, however, that recently Chernyshev [36] has considered spontaneous magnon decays of the $\boldsymbol{k} = 0$ magnon in YIG due to magnon-magnon interactions in high magnetic fields. On the experimental side, it would be useful to measure magnon damping in the exchange regime and compare the data with our theoretical prediction shown in Fig. 9.

ACKNOWLEDGMENT

Financial support by the DFG via SFB/TRR49 is gratefully acknowledged.

APPENDIX: MAGNETOELASTIC MODES FROM EQUATIONS OF MOTION

In this Appendix we show how to obtain the energy dispersions of the magnetoelastic modes from the linearized equations of motion of the coupled magnon-phonon system. Although our derivation using the effective magnon action presented in Sec. IV is simpler, the derivation in this Appendix is more in the spirit of previous work [9] using classical equations of motion.

To obtain the energy dispersions of the eigenmodes we write down the Heisenberg equations of motion of both the Holstein-Primakoff bosons and the phonon operators. Within

the linear approximation we have

$$i\dot{b}_{\boldsymbol{k}} = A_{\boldsymbol{k}} b_{\boldsymbol{k}} + B_{\boldsymbol{k}} b^{\dagger}_{-\boldsymbol{k}} + \boldsymbol{\Gamma}^{*}_{\boldsymbol{k}} \cdot \boldsymbol{X}_{\boldsymbol{k}}, \tag{A1a}$$

$$-i\dot{b}^{\dagger}_{-\boldsymbol{k}} = A_{\boldsymbol{k}} b^{\dagger}_{-\boldsymbol{k}} + B_{\boldsymbol{k}} b_{\boldsymbol{k}} + \boldsymbol{\Gamma}_{-\boldsymbol{k}} \cdot \boldsymbol{X}_{\boldsymbol{k}}, \tag{A1b}$$

$$\dot{X}_{\boldsymbol{k}\lambda} = \frac{P_{\boldsymbol{k}\lambda}}{m}, \tag{A2a}$$

$$\dot{P}_{\boldsymbol{k}\lambda} = -m\omega^{2}_{\boldsymbol{k}\lambda} X_{\boldsymbol{k}\lambda} - \Gamma_{\boldsymbol{k}\lambda} b_{\boldsymbol{k}} - \Gamma^{*}_{-\boldsymbol{k}\lambda} b^{\dagger}_{-\boldsymbol{k}}. \tag{A2b}$$

It is useful to express the equations of motion for the Holstein-Primakoff bosons in terms of the transverse spin components, which to leading order in the $1/S$ expansion can be identified with

$$S^{x}_{\boldsymbol{k}} = \frac{\sqrt{2S}}{2}(b_{\boldsymbol{k}} + b^{\dagger}_{-\boldsymbol{k}}), \tag{A3}$$

$$S^{y}_{\boldsymbol{k}} = \frac{\sqrt{2S}}{2i}(b_{\boldsymbol{k}} - b^{\dagger}_{-\boldsymbol{k}}). \tag{A4}$$

Then Eqs. (A1a) and (A1b) can be written as

$$\dot{S}^{x}_{\boldsymbol{k}} = (A_{\boldsymbol{k}} - B_{\boldsymbol{k}}) S^{y}_{\boldsymbol{k}} + i B_{\perp} \boldsymbol{k}_{yz} \cdot \boldsymbol{X}_{\boldsymbol{k}}, \tag{A5a}$$

$$\dot{S}^{y}_{\boldsymbol{k}} = -(A_{\boldsymbol{k}} + B_{\boldsymbol{k}}) S^{x}_{\boldsymbol{k}} - i B_{\perp} \boldsymbol{k}_{xz} \cdot \boldsymbol{X}_{\boldsymbol{k}}, \tag{A5b}$$

while the phonon momenta satisfy

$$\dot{P}_{\boldsymbol{k}\lambda} = -m\omega^{2}_{\boldsymbol{k}\lambda} X_{\boldsymbol{k}\lambda} + i\frac{B_{\perp}}{S} \boldsymbol{e}^{*}_{\boldsymbol{k}\lambda} \left(\boldsymbol{k}_{xz} S^{x}_{\boldsymbol{k}} + \boldsymbol{k}_{yz} S^{y}_{\boldsymbol{k}}\right), \tag{A6}$$

implying

$$\ddot{X}_{\boldsymbol{k}\lambda} + \omega^{2}_{\boldsymbol{k}\lambda} X_{\boldsymbol{k}\lambda} = i\frac{B_{\perp}}{mS} \boldsymbol{e}^{*}_{\boldsymbol{k}\lambda} \left(\boldsymbol{k}_{xz} S^{x}_{\boldsymbol{k}} + \boldsymbol{k}_{yz} S^{y}_{\boldsymbol{k}}\right). \tag{A7}$$

If we ignore the magnon-phonon coupling, we obtain from Eqs. (A5a) and (A5b),

$$\ddot{S}^{\alpha}_{\boldsymbol{k}} + E^{2}_{\boldsymbol{k}} S^{\alpha}_{\boldsymbol{k}} = 0, \quad \alpha = x, y, \tag{A8}$$

where the magnon dispersion in the absence of phonons is given in Eq. (2.9). With finite magnon-phonon hybridization we obtain the energies of the magnetoelastic modes from the roots of the secular determinant of the above equations of motion. For simplicity let us assume that the energy of only one particular phonon mode $\omega_{\boldsymbol{k}\lambda}$ is close to $E_{\boldsymbol{k}}$. To calculate the energy of the magnetoelastic mode close to the crossing point, it is then sufficient to approximate $\boldsymbol{X}_{\boldsymbol{k}} \approx X_{\boldsymbol{k}\lambda} \boldsymbol{e}_{\boldsymbol{k}\lambda}$ in the above equations of motion. Then we obtain the energies of the magnetoelastic modes from the roots of the following quartic secular equation,

$$\begin{aligned}&\left(\omega^{2} - \omega^{2}_{\boldsymbol{k}\lambda}\right)\left(\omega^{2} - E^{2}_{\boldsymbol{k}}\right) \\ &= \frac{B^{2}_{\perp}}{mS}\{(A_{\boldsymbol{k}} + B_{\boldsymbol{k}})|\boldsymbol{k}_{yz} \cdot \boldsymbol{e}_{\boldsymbol{k}\lambda}|^{2} + (A_{\boldsymbol{k}} - B_{\boldsymbol{k}})|\boldsymbol{k}_{xz} \cdot \boldsymbol{e}_{\boldsymbol{k}\lambda}|^{2} \\ &\quad + 2\omega \mathrm{Im}[(\boldsymbol{k}_{xz} \cdot \boldsymbol{e}_{\boldsymbol{k}\lambda})(\boldsymbol{k}_{yz} \cdot \boldsymbol{e}^{*}_{\boldsymbol{k}\lambda})]\}.\end{aligned} \tag{A9}$$

For the phonons in a thin YIG stripe the basis vectors $\boldsymbol{e}_{\boldsymbol{k}\lambda}$ can always be chosen such that the last term in Eq. (A9) vanishes, so that the secular equation is biquadratic and can be explicitly solved. The square of the energies of the magnetoelastic modes in a thin YIG stripe are therefore

$$(\Omega^{\pm}_{\boldsymbol{k}\lambda})^{2} = \frac{\omega^{2}_{\boldsymbol{k}\lambda} + E^{2}_{\boldsymbol{k}}}{2} \pm \sqrt{\frac{\left(\omega^{2}_{\boldsymbol{k}\lambda} - E^{2}_{\boldsymbol{k}}\right)^{2}}{4} + \Delta^{4}_{\boldsymbol{k}\lambda}}, \tag{A10}$$

where

$$\Delta^{4}_{\boldsymbol{k}\lambda} = B^{2}_{\perp}\left[(A_{\boldsymbol{k}} + B_{\boldsymbol{k}})\frac{|\boldsymbol{k}_{yz} \cdot \boldsymbol{e}_{\boldsymbol{k}\lambda}|^{2}}{mS} + (A_{\boldsymbol{k}} - B_{\boldsymbol{k}})\frac{|\boldsymbol{k}_{xz} \cdot \boldsymbol{e}_{\boldsymbol{k}\lambda}|^{2}}{mS}\right]. \tag{A11}$$

If we approximate $B_{\boldsymbol{k}} \approx 0$ (which corresponds to neglecting quantum fluctuations generated by the dipolar interaction) Eq. (A10) agrees with the result obtained via the classical equations of motion [9].

[1] See, for example, B. Lüthi, *Physical Acoustics in the Solid State* (Springer, Berlin, 2005).
[2] E. Abrahams and C. Kittel, Phys. Rev. **88**, 1200 (1952); Rev. Mod. Phys. **25**, 233 (1953).
[3] C. Kittel, Phys. Rev. **110**, 836 (1958).
[4] M. I. Kaganov and V. M. Tsukernik, Sov. Phys. JETP **9**, 151 (1959).
[5] H. F. Tiersten, J. Math. Phys. **5**, 1298 (1964).
[6] C. M. Bandari and G. S. Verma, Phys. Rev. **152**, 731 (1966).
[7] A. E. Lord, Jr., Phys. Kondens. Mater. **7**, 232 (1968).
[8] T. Kobayashi, R. C. Barker, J. L. Bleustein, and A. Yelon, Phys. Rev. B **7**, 3273 (1973).
[9] A. G. Gurevich and G. A. Melkov, *Magnetization Oscillations and Waves* (CRC, Boca Raton, FL, 1996).
[10] L. Dreher, M. Weiler, M. Pernpeintner, H. Huebl, R. Gross, M. S. Brandt, and S. T. B. Goennenwein, Phys. Rev. B **86**, 134415 (2012).
[11] A. Kamra and G. E. W. Bauer, Solid State Commun. (2013).
[12] M. Agrawal, V. I. Vasyuchka, A. A. Serga, A. D. Karenowska, G. A. Melkov, and B. Hillebrands, Phys. Rev. Lett. **111**, 107204 (2013).
[13] K. Uchida, S. Takahashi, K. Harii, J. Ieda, W. Koshibae, K. Ando, S. Makawa, and E. Saitoh, Nature (London) **455**, 778 (2008).
[14] C. W. Sandweg, M. B. Jungfleisch, V. I. Vasyuchka, A. A. Serga, P. Clausen, H. Schultheiss, B. Hillebrands, A. Kreisel, and P. Kopietz, Rev. Sci. Instrum. **81**, 073902 (2010).
[15] V. Cherepanov, I. Kolokolov, and V. L'vov, Phys. Rep. **229**, 81 (1993).
[16] I. S. Tupitsyn, P. C. E. Stamp, and A. L. Burin, Phys. Rev. Lett. **100**, 257202 (2008).
[17] A. Kreisel, F. Sauli, L. Bartosch, and P. Kopietz, Eur. Phys. J. B **71**, 59 (2009).
[18] T. Holstein and H. Primakoff, Phys. Rev. **58**, 1098 (1940).
[19] B. A. Kalinikos and A. N. Slavin, J. Phys. C **19**, 7013 (1986); J. Phys. Condens. Matter **2**, 9861 (1990).
[20] M. A. Gilleo and S. Geller, Phys. Rev. **110**, 73 (1958).
[21] A. Kreisel, P. Kopietz, P. T. Cong, B. Wolf, and M. Lang, Phys. Rev. B **84**, 024414 (2011).
[22] F. G. Eggers and W. Strauss, J. Appl. Phys. **34**, 1180 (1963).
[23] P. Hansen, Phys. Rev. B **8**, 246 (1973).

[24] To satisfy $\boldsymbol{e}^*_{\boldsymbol{k}\lambda} = \boldsymbol{e}_{-\boldsymbol{k}\lambda}$ one should set $\boldsymbol{e}_{\boldsymbol{k}\lambda} = i\hat{\boldsymbol{k}}$ for longitudinal modes; see M. P. Marder, *Condensed Matter Physics* (Wiley, New York, 2000), p. 316 for a discussion of this point.

[25] J. Hick, T. Kloss, and P. Kopietz, Phys. Rev. B **86**, 184417 (2012).

[26] M. G. Cottam and D. J. Lockwood, *Light Scattering in Magnetic Solids* (Wiley, New York, 1986).

[27] J. Jorzick, S. O. Demokritov, C. Mathieu, B. Hillebrands, B. Bartenlian, C. Chappert, F. Rousseaux, and A. N. Slavin, Phys. Rev. B **60**, 15194 (1999).

[28] S. O. Demokritov, V. E. Demidov, O. Dzyapko, G. A. Melkov, A. A. Serga, B. Hillebrands, and A. N. Slavin, Nature (London) **443**, 430 (2006).

[29] V. E. Demidov, O. Dzyapko, M. Buchmeier, T. Stockhoff, G. Schmitz, G. A. Melkov, and S. O. Demokritov, Phys. Rev. Lett. **101**, 257201 (2008).

[30] A. A. Serga, C. W. Sandweg, V. I. Vasyuchka, M. B. Jungfleisch, B. Hillebrands, A. Kreisel, P. Kopietz, and M. P. Kostylev, Phys. Rev. B **86**, 134403 (2012).

[31] M. Sparks, *Ferromagnetic-Relaxation Theory* (McGraw-Hill, New York, 1964).

[32] A. V. Chumak, A. A. Serga, B. Hillebrands, G. A. Melkov, V. Tiberkevich, and A. N. Slavin, Phys. Rev. B **79**, 014405 (2009).

[33] A. V. Chumak, A. A. Serga, M. B. Jungfleisch, R. Neb, D. A. Bozhko, V. S. Tiberkevich, and B. Hillebrands, Appl. Phys. Lett. **100**, 082405 (2012).

[34] M. J. Hurben and C. E. Patton, J. Appl. Phys. **83**, 4344 (1998).

[35] B. Hillebrands *et al.*, Annual Report 2012: http://www.physik.uni-kl.de/hillebrands/publications/annual-reports/annual-report-2012.

[36] A. L. Chernyshev, Phys. Rev. B **86**, 060401(R) (2012).